Eur. J. Mineral., 36, 767–795, 2024
https://doi.org/10.5194/ejm-36-767-2024

European Journal of Mineralogy
Open Access

High-pressure Ca metasomatism of metabasites (Mont Avic, Western Alps): insights into fluid–rock interaction during subduction

Kilian Lecacheur[1], Olivier Fabbri[1], Francesca Piccoli[2], Pierre Lanari[2,3], Philippe Goncalves[1], and Henri Leclère[1]

[1]Chrono-environnement, UMR CNRS 6249, Université de Franche-Comté, 16 route de Gray, 25000 Besançon, France
[2]Institute of Geological Sciences, University of Bern, Baltzerstrasse 1 + 3, 3012 Bern, Switzerland
[3]Institute of Earth Sciences, University of Lausanne, Géopolis, 1005 Lausanne, Switzerland

Correspondence: Kilian Lecacheur (kilian.lecacheur@univ-fcomte.fr)

Received: 8 September 2023 – Revised: 21 June 2024 – Accepted: 15 July 2024 – Published: 12 September 2024

Abstract. The study of rock chemistry is a milestone in understanding fluid–rock interactions and fluid migration in subduction zones. When combined with thermodynamic models, it can provide direct insight into fluid composition, metasomatic reactions, and pressure–temperature (P–T) conditions, as well as their role in rock deformation. Here, a shear zone – located in the Mont Avic area of the Zermatt-Saas zone (Western Alps) – is analyzed. This shear zone consists of several blocks of different lithotypes, including a Ca-rich metasomatite block embedded in a serpentinite mylonitic matrix, and structurally underlies a coherent eclogitic mafic unit. This work aims to estimate the pressure–temperature conditions of the Ca-rich metasomatism and the amount of fluid involved. The brecciation exhibits mosaic breccia textures with clasts comprising ~ 80 vol % of garnet, together with omphacite, epidote, titanite, rutile, and apatite hosted in an omphacite matrix. Quantitative chemical mapping of the garnet reveals primary garnet cores with embayment and lobate edges with a chemical composition similar to unaltered reference eclogite garnet. These primary garnet cores are overlain by Ca-rich metasomatic garnet rims with oscillatory chemical zoning. The oscillatory chemical zoning, together with the morphology of the primary garnet cores, suggests repeated influxes of external Ca-rich fluid that destabilized the primary garnet cores and promoted the growth of Ca-rich rims. Mass balance calculations between precursor metabasite and Ca-metasomatite indicate multiple fluid sources involving dehydrated serpentinite, calcic metasediments, and metabasites with time-integrated fluid fluxes calculated between 11.5×10^3 and 5.5×10^4 m^3_{fluid} m^{-2}_{rock}, consistent with channelized fluid flow in an open system. Thermodynamic modeling of garnet from unbrecciated and non-metasomatized metabasites – from the Savoney eclogitic mafic unit – indicates peak metamorphic conditions of 2.5 ± 0.1 GPa and 535 ± 40 °C, consistent with regional estimates. Pressure–temperature conditions of metasomatism were constrained using P–X and T–X phase modeling (where X represents changes in bulk CaO and Na_2O composition) between 2.6–2.2 GPa and 570–500 °C, showing that Ca-rich fluid percolation occurred close to the metamorphic peak (i.e., prograde to the peak or early exhumation path).

1 Introduction

Large quantities of fluids are released in subduction zones by progressive dehydration of the downgoing oceanic lithosphere (Hacker et al., 2003; Schmidt and Poli, 2013). Fluid release from the subducted oceanic crust has significant implications for metamorphic re-equilibration, intermediate-depth seismicity (Philippot, 1987; Angiboust et al., 2012a; Malvoisin et al., 2015; Locatelli et al., 2018; Plümper et al., 2017), geochemical cycling (Bebout and Barton, 1993; Bebout, 2013; Angiboust et al., 2014b; Piccoli et al., 2016; Herviou and Bonnet, 2023), and the generation of sub-arc magmatism (Schmidt and Poli, 1998). Despite the recent increase in geophysical and petrological evidence for fluid circulation along subducting slab interfaces in high-pressure terranes, retrogression and deformation can obscure field evidence of fluid–rock interactions. Nevertheless, field evidence of fluid flow under high-pressure conditions is critical for a better understanding of subduction zones' geochemical cycling and the rheological–hydraulic properties that regulate flow (Connolly and Podladchikov, 2007; Connolly, 2010; Faccenda et al., 2012; Maggi et al., 2014; Wilson et al., 2014; Bedford et al., 2017; Giuntoli et al., 2020; Piccoli et al., 2021).

Metamorphic fluids play an important role as metasomatic agents of slab-forming rocks during their upward migration toward the mantle wedge (Bebout and Barton, 2002; Breeding et al., 2004; Martin et al., 2011, 2014; Angiboust et al., 2012b, 2014a, 2017; Rubatto and Angiboust, 2015; Gerrits et al., 2019; Gyomlai et al., 2021) and leave a geochemical and isotopic signature in the reacting minerals. If equilibration between the fluid and the system is incomplete, a record of the previous metamorphic stages is preserved in relict minerals (Lanari and Engi, 2017). Garnet is an exceptional mineral for tracking transient states and chemical changes during fluid–rock interactions because it is present in most metamorphic rocks and is stable under a wide range of metamorphic conditions. Moreover, due to the low intracrystalline diffusion rate below 700 °C, garnet may preserve distinct chemical compositional zoning corresponding to various metamorphic stages (Spear, 1991; Carlson and Gordon, 2004; Konrad-Schmolke et al., 2006; Caddick et al., 2010; Ague and Carlson, 2013). Typical garnet growth during a prograde path is defined by bell-shaped zoning (for major and trace elements) regulated by Rayleigh fractionation (Hollister, 1966; Atherton, 1968; Cygan and Lasaga, 1982; Evans, 2004; Moore et al., 2013). However, the reaction with an external fluid could lead to partial dissolution of garnet and reprecipitation of a new garnet with a different chemical composition. In this case, the prograde metamorphic garnet will be constituted with resorption textures surrounded by the new metasomatic garnet (Schumacher et al., 1999; García-Casco et al., 2002; Konrad-Schmolke et al., 2007; Angiboust et al., 2011, 2017; Ruiz Cruz, 2011; Giuntoli et al., 2018b). Moreover, the analysis of metasomatic reactions using bulk-rock and mineral chemistry can provide critical information about the source, composition, and quantity of percolating fluids and the mechanisms of fluid transfer.

The Zermatt-Saas ophiolite complex in the Western Alps is an exceptional natural laboratory for the investigation of eclogite-facies rocks metamorphosed in a subduction setting. This contribution focuses on a Ca-metasomatite from a shear zone in the Mont Avic area, in the southern part of the Zermatt–Saas zone (ZSZ). We describe and compare microstructural and mineral chemical composition from the Ca-metasomatite with a reference eclogite with a typical high-pressure (HP) mineral assemblage from a nearby coherent unit. These observations are combined with mass balance calculation and thermodynamic modeling to decipher the pressure–temperature (P–T) conditions of the formation of the Ca-metasomatite, quantify mass transfer, and investigate the role of fluid–rock interactions in phase relations. These results are combined to estimate the quantity of fluids and discuss possible sources.

2 Geological setting

The Zermatt-Saas zone (ZSZ) belongs to the south Penninic nappe stack system in the internal Western Alps (Fig. 1). It is a remnant of the Jurassic (160–120 Ma) Piemont-Ligurian oceanic lithosphere and was buried down to 80–100 km during the Alpine subduction in Cretaceous to Eocene times beneath the Apulian margin (Lemoine et al., 1986; Bowtell et al., 1994; Rubatto et al., 1998; Amato et al., 1999). The oceanic crust of the Alpine Tethys in the Western Alps is constituted of serpentinites, metasediments, metabasalts, and metagabbros, as well as, to a lesser extent, metarodingites. During the Alpine collision in mid-Tertiary times, the ZSZ was exhumed together with ultra-high-pressure (UHP) continental units of the European stretched margin, resulting in a dome structure with the ZSZ wrapping the European continental basement (Schmid et al., 2004). The ZSZ also includes kilometer-scale klippen or thrust sheets of Austroalpine continental slices (Monte Emilius, Glacier–Rafray, the Theodul Glacier unit, Etirol–Levaz, and so on) intercalated in ophiolitic thrust sheets (Dal Piaz and Nervo, 1971; Ballèvre et al., 1986; Dal Piaz et al., 2001; Weber and Bucher, 2015; Fassmer et al., 2016). These continental slivers are interpreted as former extensional allochthons derived from the stretched Apulian continental margin and subsequently subducted together with the oceanic lithosphere (Dal Piaz et al., 2001; Beltrando et al., 2014). During the Alpine subduction, the ZSZ first followed a prograde path that culminated in eclogitic conditions (Reinecke, 1991) and was then metamorphosed under blueschist- to greenschist-facies conditions along a retrograde path during exhumation (Bearth, 1967; Ernst and Dal Piaz, 1978; Cartwright and Barnicoat, 2002). The ZSZ oceanic rocks were affected by oceanic metasomatism, resulting in the serpentinization of the mantle peri-

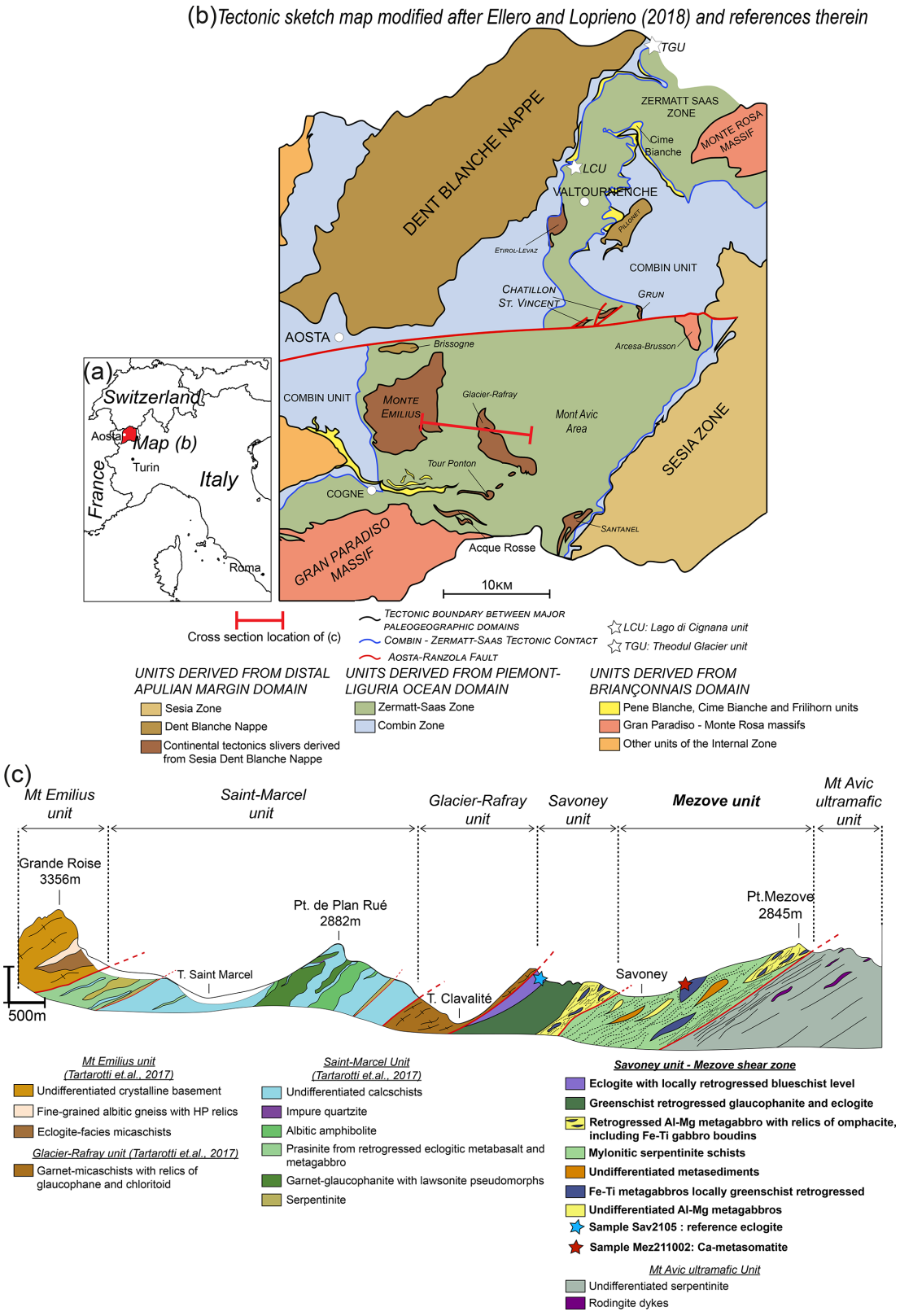

Figure 1. Geological setting of the studied area. **(a)** Location of the study area. **(b)** Tectonic sketch of the eastern Aosta Valley area modified after Ellero and Loprieno (2018). **(c)** Cross section across the study area (red line in **b** with sample locations (Sav2105: 45°39′21.84″ N, 7°30′40.58″ E; Mez211002: 45°39′14.79″ N, 7°31′54.76″ E)). The Saint-Marcel unit and the Monte Emilius slice were redrawn according to the cross section of Tartarotti et al. (2017a) with the addition of slices based on the work of Angiboust and Agard (2010).

dotites and rodingitization of gabbroic intrusions in the mantle section (Li et al., 2004; Zanoni et al., 2016).

To the south of the E–W Aosta–Ranzola late-orogenic normal fault, the ZSZ is widely exposed in the Mont Avic area (Fig. 1). It consists of a ca. 200 km^2 body of ultramafic rocks (Mont Avic ultramafic unit) surrounded by metabasites, metasediments, and continental slivers. The ultramafic rocks consist of variously foliated serpentinites that locally include lenses of Al–Mg and Fe–Ti metagabbros and dikes of metarodingites (Tartarotti et al., 1998; Fontana et al., 2008, 2015; Panseri et al., 2008). The serpentinite in contact with the gabbro lenses is strongly foliated and can be referred to as a serpentinite schist. Despite a pervasive foliation, the secant contacts between metarodingitic dikes and the host serpentinite can be recognized. The western part of the Mont Avic area consists of a west-dipping stack of thrust sheets which are, from west to east, the Monte Emilius unit, the Saint-Marcel unit, the Glacier–Rafray unit, the Savoney unit, the Mezove unit, and the uppermost part of the Mont Avic ultramafic unit (Fig. 1). The Saint-Marcel unit corresponds to the uppermost oceanic crust and consists of metasediments (calc-schists, metacherts), metatuffs, and metabasalts (Tartarotti et al., 2017b). Metabasalts locally show relicts of pillow structures. The Mezove unit, which is the focus of this study, consists of foliated serpentinite with lenses of eclogitic Fe–Ti or Al–Mg metagabbros and glaucophanite. Glaucophanite likely corresponds to metamorphosed basalts and is composed of a high lawsonite pseudomorph content with eclogitic boudins (Angiboust and Agard, 2010).

Metabasites and serpentinites within the Zermatt-Saas zone (ZSZ) underwent high-pressure (HP) to ultra-high-pressure (UHP) conditions during the Alpine subduction event. North of the Aosta–Ranzola fault, in the Zermatt area, metagabbros and metabasalts experienced peak conditions at 2.3–3.0 GPa and 530–650 °C (Bucher et al., 2005; Angiboust et al., 2009; Groppo et al., 2009), while serpentinite and associated rodingite from the Valtournenche area recorded conditions of 2.2–2.8 GPa and 580–660 °C (Rebay et al., 2012; Zanoni et al., 2016; Luoni et al., 2019). Coesite and micro-diamond inclusions in metabasites and metasedimentary rocks within the Lago di Cignana unit indicate UHP conditions at 3.2 GPa and 600 °C (Reinecke, 1991, 1998; Van Der Klauw et al., 1997; Groppo et al., 2009). In the Saint-Marcel unit, south of the Aosta–Ranzola fault, metabasites exhibit peak conditions at 2.1–2.3 GPa and 520–560 °C (Martin et al., 2008; Angiboust et al., 2009; Dragovic et al., 2020). Similar conditions are observed by Angiboust et al. (2009) in metabasites in the easternmost part of the Mont Avic area. The P–T estimates and the prograde path constrain the ZSZ in the lawsonite stability field for metabasites and metasediments (Angiboust et al., 2009; Angiboust and Agard, 2010) and indicate that the ultramafic rocks of the unit crossed the brucite breakdown reaction which occurs at 2–2.5 GPa and 480–550 °C (Scambelluri et al., 1991; Ulmer and Trommsdorff, 1999; Bretscher et al., 2018; Kempf et al., 2020). The brucite dehydration reaction can occur within a narrow temperature interval, and such a focused fluid release can potentially trigger intermediate-depth seismicity (Kempf et al., 2020). High-pressure assemblages in the Mont Avic serpentinite include antigorite + magnetite + chlorite + amphibole + clinopyroxene + Ti-clinohumite + olivine. Ti-clinohumite + olivine + clinopyroxene veins were initially proposed to have formed at mid-oceanic ridges and recrystallized under eclogite-facies conditions during subduction (Fontana et al., 2008). More recently, these veins, also observed in the northern ZSZ, were considered to result from serpentinite dehydration under HP or UHP conditions (Luoni et al., 2019; Gilio et al., 2020; Kempf et al., 2020). Considering the high Mn content of the olivine and the textural similarities with the brucite-out dehydration veins from the broader Zermatt-Saas unit as well as from the Erro–Tobbio unit (Scambelluri et al., 1991, 1995), we suggest that the Mont Avic olivine + Ti-clinohumite veins are also derived from the partial dehydration of the serpentinites.

3 Methods

3.1 Bulk-rock chemistry

Bulk-rock chemical analyses were acquired using a PANalytical Axios^{mAX} X-ray fluorescence (XRF) spectrometer at the University of Lausanne, Switzerland. Quality control was tested with BHVO-2 and JA-3 reference materials for major elements (Jochum et al., 2016).

The Sav2105 sample is composed of less than 10 % carbonate phases. For a better estimate of the peak metamorphic conditions, the CO_2 phases were subtracted and a reactive bulk-rock composition was recalculated using the method of Lanari and Engi (2017).

3.2 Mass balance calculation

Mass balance and volume change calculations are based on the method from Ague (1994, 2011), Ague and Van Haren (1996), and Philpotts and Ague (2009). The calculation is made with the assumption that the mass of an immobile element is constant during volume change. During alteration or metasomatism, the enrichment or depletion of elements leads to variations in the mass and volume of the rock. The quantification of the change in rock mass ($T_{\mathrm{mass},i}$), which is determined by considering an immobile reference species c_i and a mobile species c_j, can be expressed as follows:

$$T_{\mathrm{mass},i} = \frac{c_i^0}{c_j^{\mathrm{A}}} - 1.$$

The percentage mass change is obtained by multiplying $T_{\mathrm{mass},i}$ by 100. The superscripts ^{0} and ^{A} denote the precursor and altered rock, respectively. In the case where the rock

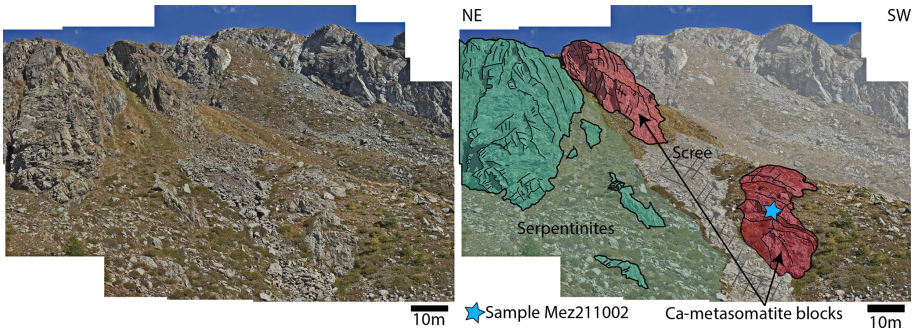

Figure 2. Outcrop photographs of the Ca-metasomatite blocks (red) embedded in the foliated serpentinite matrix (green). The blue star indicates the location of the Mez211002 sample.

mass has decreased, the concentration of species i in the altered rock will be higher than in the protolith, indicating a residual enrichment of i. Conversely, if rock mass has increased, the mass of species i in the altered rock will be lower than in the protolith, indicating residual dilution of i.

The fractional mass change in a mobile species j estimated using the reference immobile species i is

$$\tau_i^j = \left(\frac{c_i^0}{c_i^A}\right)\left(\frac{c_j^A}{c_j^0}\right) - 1,$$

where indices c_i comprise the mass fraction of the reference component i and c_j is the mass fraction of j.

For the calculation, we assume that Zr is the least mobile element and has an extremely low solubility in HP fluids (Ayers and Watson, 1991; Breeding et al., 2004) and we use the mean reference eclogite bulk as the unaltered rock and the mean Ca-metasomatite as the altered rock (Table 3). The Zr composition ranges from 94.6 µg g^{-1} for the reference eclogite to 102.6 µg g^{-1} for the Ca-metasomatite (Table S1 in the Supplement).

The overall rock volume strain (ε_i) using a reference species i is given by

$$\varepsilon_i = \left(\frac{c_i^0}{c_i^A}\right)\left(\frac{\rho^0}{\rho^A}\right) - 1,$$

where ρ^0 and ρ^A are the precursor and metasomatic rock density, respectively. Here, we model rock densities using the software Perple_X (version 6.9.1) (Connolly, 2005) with the internally consistent thermodynamic database of Holland and Powell (2011).

3.3 SEM and EPMA analyses

Backscattered electron (BSE) images were acquired using an Apreo S scanning electron microscope (MIMENTO FEMTO-ST, University of Franche-Comté) with a 20 kV acceleration voltage and a 3.2 nA current beam. Quantitative analyses were performed with the electron probe microanalyzer (EPMA) JEOL JXA-8200 superprobe at the Institute of Geological Sciences, University of Bern, Switzerland. Spot analyses were performed using a 15 kV accelerating voltage, a 20 nA specimen current, and a 40 s dwell time. Nine oxide components were acquired using synthetic and natural standards: garnet (SiO_2, Al_2O_3, FeO, and MnO), albite (Na_2O), anorthite (CaO), orthoclase (K_2O), forsterite (MgO), and ilmenite (TiO_2). Quantitative compositional maps were produced from intensity maps using spot analyses of the same area as internal standards. Compositional maps were processed using XMapTools 4 (Lanari et al., 2014, 2019). Structural formulas for garnet, omphacite, epidote, and amphibole were calculated using the external functions available in XMapTools.

3.4 Thermodynamic modeling

Pressure–temperature (P–T) and temperature–composition (T–X) phase diagrams were calculated in the Na_2O–CaO–FeO–MgO–Al_2O_3–SiO_2–H_2O–TiO_2–Fe_2O_3 (NCFMASHTi) system using the Perple_X 6.9.1 software (Connolly, 2005) and the thermodynamic database ds62 from Holland and Powell (2011). The equation of state used for H_2O is from Holland and Powell (1998). All the phase diagrams were computed assuming fluid-saturated conditions to promote mass transfer. Fluid is assumed to be pure H_2O.

Mineral solution models used in the calculations are those of White et al. (2014; chlorite, white mica, and garnet), Holland and Powell (2011; epidote), Holland and Powell (2003; feldspar), Green et al. (2016; amphibole and omphacite), and White et al. (2000; ilmenite); all other minerals involved in the calculations were considered pure phases.

Based on the chemical composition of omphacite containing 12 %–14 % of aegirine, garnet containing 2 %–3 % of andradite, and the modal amount of lawsonite that is dependent on the Fe^{3+} content in the bulk-rock compositions (Angiboust and Agard, 2010), we created P–X and T–X diagrams, with X standing for the increasing in Fe^{3+} in the system. The Fe^{3+} in the bulk composition was set at 0.17 for the Sav2105

sample and at 0.27 for the Mez211002 sample (Fig. S1 in the Supplement).

4 Results

4.1 Field structural observations

The analyzed samples Sav2105 and Mez211002 belong to the Savoney and Mezove units, respectively (Fig. 1b, c). The Sav2105 sample is from a coherent hectometric eclogitic metabasite body located at the top of the Savoney unit, approximately 200 m below the tectonic contact with the Glacier–Rafray unit (Fig. 1c). The Sav2105 sample is considered the reference eclogite for the study area. The reference eclogite was not sampled in the Mezove unit because most blocks in this unit were probably affected by fluid–rock interactions and are highly retrogressed.

Below the Savoney unit, the Mezove unit is a shear zone consisting of foliated serpentinite and meter- to decameter-scale lenses of blueschist to eclogitic Fe–Ti metagabbros, Al–Mg metagabbros, metabasites, and metasediments. Eclogitic metabasites are former basalts or Fe–Ti gabbros (Fig. 1c). Wherever eclogitic metabasite lenses are embedded in Al–Mg metagabbro, they are interpreted as ancient dikes, sills, or igneous enclaves. The metabasite lenses are partly retrogressed in blueschist- to greenschist-facies conditions, but the eclogitic assemblage is preserved in most lenses. The four samples Mez211002(A), Mez211002(B), Mez211003, and Mez220801 are from the inner part of a decameter-long eclogitic metabasite block surrounded by foliated serpentinite (Fig. 2). A 10 cm thick chlorite-rich blackwall develops at the contact between the lens and the host serpentinite. The brecciation structure is visible in the inner part of the lens, while the outer part of the lens preserves the eclogitic structure without brecciation (Fig. 4a, b). The transition between the inner brecciated part and the outer non-brecciated part is not exposed.

4.1.1 Petrology of the studied samples

To facilitate the description of the reference eclogite and the Ca-metasomatite, we define three metamorphic stages and their mineral assemblages as follows (Grt, garnet; Omp, omphacite; Ep, epidote): the M1 eclogitic stage with Grt1, Omp1, and Ep1; the M2 Ca-metasomatite stage with Grt2, Omp2, and Ep2; and the late M3 stage with only Omp3. Comparison and interpretation of the two first stages are discussed in Sect. 5.1.

4.1.2 Reference eclogite (Sav2105)

The reference eclogite is a weakly retrogressed metabasite composed of garnet (40 vol %) and omphacite (40 %), with rutile (5 %), aggregates of epidote (5 %), blue amphibole (2 %), and dolomite (8 %). The constitutive minerals do not show any preferred orientation (Fig. 3a).

Omphacite occurs as coarse anhedral grains that do not exceed 1 mm in size. It is not chemically zoned and has a homogeneous composition of Jd_{37}–Di_{36}–Aeg_{16-17}–Hd_{10} (Jd, jadeite; Di, diopside; Aeg, aegirine; Hd, hedenbergite) (Table 1, Fig. 6b).

Garnet is sub-euhedral with a grain size between 500 µm and 2 mm. The inner core contains inclusions of glaucophane and epidote, while the outer core contains inclusions of rutile, ilmenite, epidote, and omphacite (Fig. 3b). Garnet is chemically zoned, with a high content of Mn and Ca in the core, and a Fe–Mg-enriched rim (Fig. 3). The Mn content variation across the garnet exhibits a bell-shaped profile, with composition ranging from Alm_{45}–Grs_{32}–Sps_{18}–Prp_3–And_2 (Alm, almandine; Grs, grossular; Sps, spessartine; Prp, pyrope; And, andradite) in the inner part of the core to Alm_{62}–Grs_{30}–Sps_1–Prp_4–And_3 in the outer part of the core and to Alm_{60}–Grs_{25}–Sps_1–Prp_{11}–And_4 in the outermost rim (Figs. 3 and 6, Table 1).

Epidote is present in the sample with random or losangic aggregates and is also abundant as inclusions in garnet. The composition of epidote in aggregates is Ep_{71}–Zo_{28} (Zo denotes zoisite).

Amphibole occurs as sub-idiomorphic grain aggregates associated with omphacite. It mostly consists of Na-amphibole, with 85 % glaucophane content (Table 1). Rutile appears as random aggregates or trails in the matrix (Fig. 3a). Rutile is also present as inclusions in the outer core of the Grt1 (Fig. 3a, b). Carbonates with idiomorphic shapes are present with omphacite and other minerals but are not present as inclusions in Grt1 (Fig. 3a).

4.1.3 Ca-metasomatite (Mez 211002)

The Mez211002 sample comes from the inner brecciated part of the eclogitic metabasite lens. Polished saw-cut sections in Fig. 4a and b show that the breccia is a mosaic breccia following the terminology of Woodcock and Mort (2008). Clasts are not in contact but are separated by an omphacite matrix and show minor rotations of less than 10°. The surface percentage of clasts is between 60 % and 70 %. The size of the clasts ranges from 1 cm to less than 1 mm (Fig. 4). When clasts are less than 1 mm, they mostly consist of fragmented garnet pieces (Fig. 5d). Large clasts are sub-angular to rounded and are cemented by an omphacite matrix. The contact between the clasts, whatever their size and the matrix, is sharp (Fig. 4c, d). The clasts are constituted of 60 vol %–80 vol % of garnet, showing a garnetite-like texture. Inside the clasts, garnet shows an idiomorphic shape. The garnet shows an equilibrium texture with apatite, titanite, epidote, omphacite (Omp2), and rutile. Several garnet grains show atoll-like textures with a concentric garnet rim filled mostly with omphacite and less frequently with epidote and titanite.

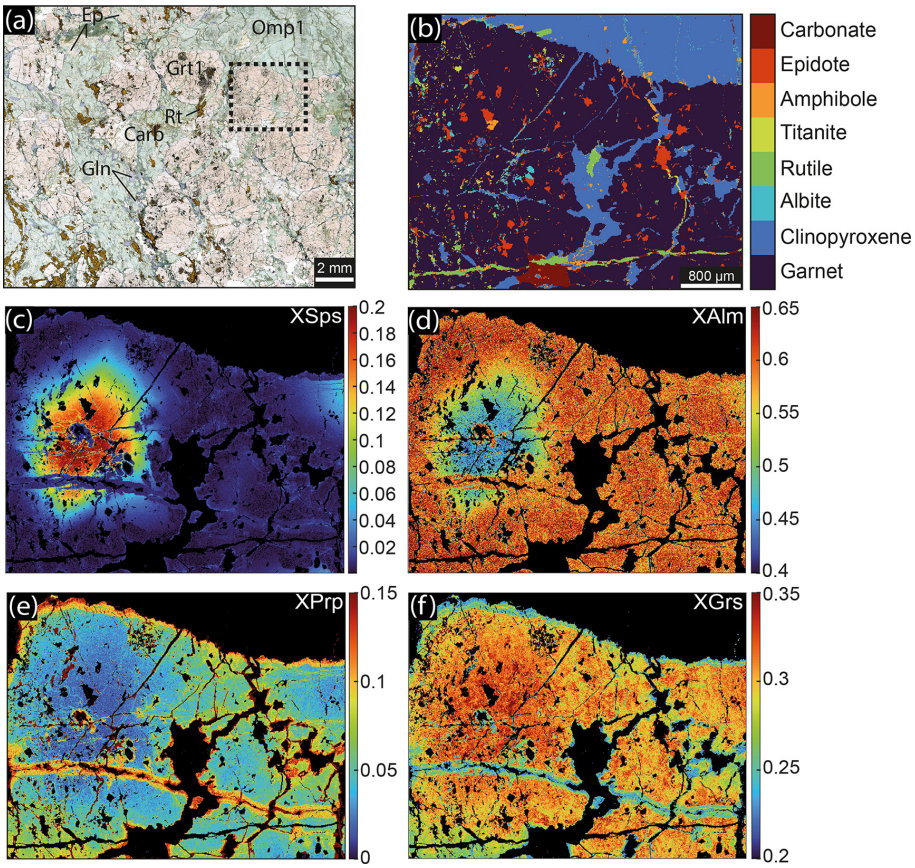

Figure 3. Petrology of the reference eclogite Sav2105. **(a)** Plane-polarized light photomicrograph showing the principal mineral assemblage of Grt1 + Omp1 + Rt + Gln + Ep (Lws pseudomorphs) + Carb (Gln, glaucophane; Lws, lawsonite; Carb, carbonate). The dotted black square indicates the position of the EPMA map of **(c)** to **(f)**. **(b)** Mineral map obtained after classification of the X-ray maps. **(c–f)** Chemical maps of the fraction of spessartine (XSps), almandine (XAlm), pyrope (XPrp), and grossular (XGrs).

Island or peninsula garnets are also preserved inside the atoll garnets (Figs. 5c and d and 7).

Backscattered electron (BSE) images reveal three generations of garnet. Grt1 is characterized by lobate structures filled with peninsulas surrounded by a second-generation garnet Grt2 (Figs. 7 and 8). The BSE image of Fig. 5e and the XPrp and XSps maps of Fig. 8 show that Grt1 is crossed by a network of fractures sealed by another garnet generation. Compared to Grt1, the sealing garnet is enriched in Mg and depleted in Mn. Grt1 is isolated from the matrix by the surrounding Grt2. Grt2 is the most abundant garnet generation and surrounds Omp2, titanite, or epidote and has an atoll-like morphology. The main feature of Grt2 is the occurrence of an oscillatory zoning pattern (Figs. 7 and 8). In many cases, Grt2 is surrounded by a third generation of garnet (Grt3), which is characterized by the absence of any chemical zoning and has a homogeneous composition (Figs. 6 and 7). Grt1 has the same composition as the prograde metamorphic garnet of the reference eclogite. The inner core of Grt1 is enriched in Mn and Ca (Fig. 6a, Table 2) (Alm_{47}–Grs_{25}–Sps_{20}–Prp_{02}–And_{04}), while the outer core is enriched in Fe and depleted in Mn (Alm_{54}–Grs_{27}–Sps_{09}–Prp_{03}–And_{06}). The transition between the two domains is diffuse (Figs. 7 and 8). A striking chemical feature of Grt2 is the Ca content, which is 20 %–30 % higher than in Grt1 and reaches up to 55 % of XGrs. Figure 7 shows various patterns of oscillatory zoning in Grt2. The oscillatory zoning pattern of the rims follows the lobate structure of the garnet core. The innermost zoned rim of Grt2, referred to as Grt2a, is in contact with Grt1, with Omp2, or with titanite + epidote, and it has the highest Ca content and the lowest Fe content (Fig. 6a, Table 2), Alm_{39}–Grs_{54}–Prp_{04}–Sps_{02}–And_{02}. The second rim is characterized by a Ca decrease and a Fe increase (Fig. 6a), Alm_{50}–Grs_{41}–Prp_{06}–Sps_{01}–And_{04}. The Ca and Fe contents are similar in the third rim, and the composition is Alm_{47}–Grs_{42}–Prp_{08}–Sps_{01}–And_{03} (Fig. 6a). The last Grt2 rim is again characterized by an increase in Fe and a decrease in Ca (Fig. 6a), Alm_{50}–Grs_{38}–Sps_{00}–Prp_{05}–And_{06}. The Ca content of omphacite included in garnet (Omp2: Jd_{20}–Di_{54}–Aeg_{14}–Hd_{12}) is higher than in the matrix omphacite. For this reason, we distinguish omphacite 2 (Omp2), included in garnet from matrix omphacite 3 (Omp3:

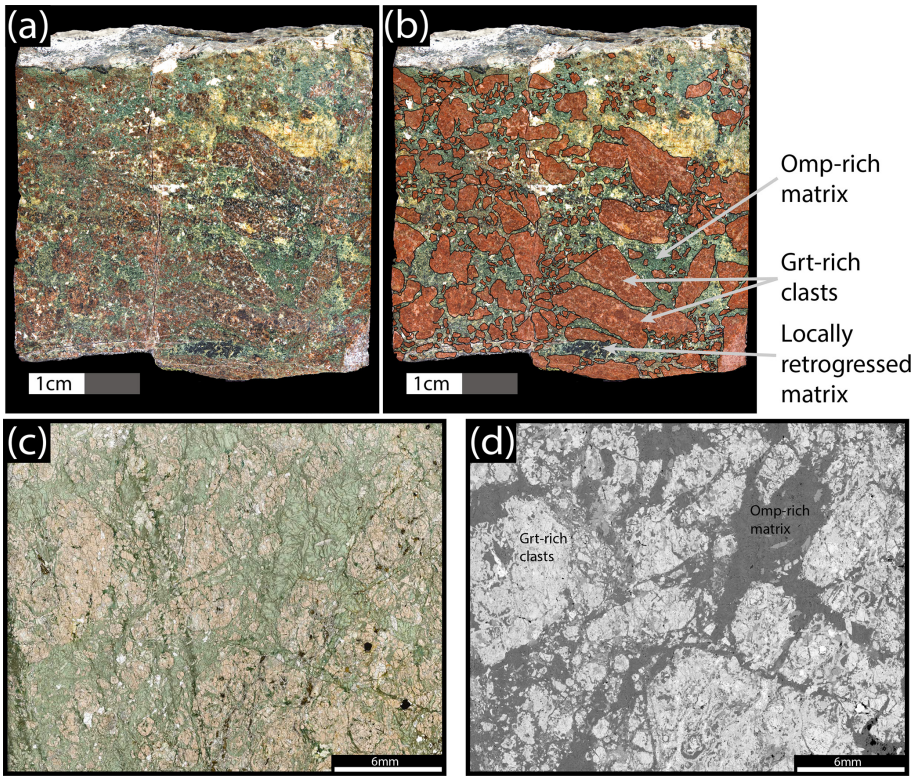

Figure 4. **(a)** Hand-polished sample sections of metasomatic eclogite breccia (Mez211002). Mosaic-supported breccia showing sub-angular to rounded clasts of metasomatic eclogite and omphacitic (Omp2) matrix. The matrix is locally retrogressed. The yellow mass in the upper-right corner is epidote (lawsonite pseudomorph). **(b)** Sketch of **(a)**. **(c)** Thin-section scan showing large (centimeter-scale) sub-angular to rounded clasts and smaller (millimeter-scale) angular clasts (horizontal length: 30 mm). The greenish matrix mainly consists of omphacite (Omp3). The rectilinear planes cross-cutting the section from top left to bottom right are late fractures along with chlorite and epidote replacing omphacite. **(d)** BSE image of the area of **(b)**.

Jd_{26}–Di_{49}–Aeg_{15}–Hd_{10}; Table 2; Fig. 6b), composed of subeuhedral grains with elongated tabular shapes. Both Ca-rich Grt2 and Omp2 appear in textural equilibrium with other Ca-rich minerals such as apatite, titanite, and calcic epidote. The Omp3 includes fragments of titanite, garnet, apatite, and epidote. The fragments are angular with sizes between less than 100 µm and about 1 mm (Fig. 5). The vein network in the matrix shows omphacite grains elongated perpendicularly to the clasts (Fig. 5c).

Epidote is anhedral and associated with omphacite and apatite inside and outside atoll-shaped garnets. Epidote is also visible in the matrix but with tabular or angular shapes (Fig. 5). The chemical composition of epidote ranges from Ep_{60}–Zo_{38} to Ep_{65}–Zo_{35} (Table 2). Rutile is found as tails or aggregates always surrounded by titanite. Titanite is associated with the mineral assemblage composing the clasts. Figure 5c shows that titanite could grow around garnet or with a euhedral shape.

4.2 Mass balance analysis

The bulk compositions of the reference eclogite are close to a MORB composition, similar to eclogites in the ZSZ (Fig. 9a, Table 3). The bulk composition of the Ca-metasomatite sample has a higher Ca content and a lower Na content and plots close to metarodingite compositions.

For the mass balance calculation, an average bulk composition for the Ca-metasomatite was calculated from four samples for major elements and one for trace elements (Tables 3, S1). For the reference eclogite, the average bulk composition in major elements was calculated from two samples, and only one bulk was used for the trace elements (Tables 3, S1). The four Ca-metasomatite samples come from the same outcrop (Fig. 2). The two samples of reference eclogite come from the Savoney unit. Due to the small number of samples, statistical uncertainty cannot be calculated. Therefore, for trace elements that show significant variability in the mass fraction between samples, we report only the minimum mass change value to provide a conservative estimate. The first result of the mass balance analysis shows that considering a density of 3650 kg m^{-3} for the reference eclogite and 3673 kg m^{-3}

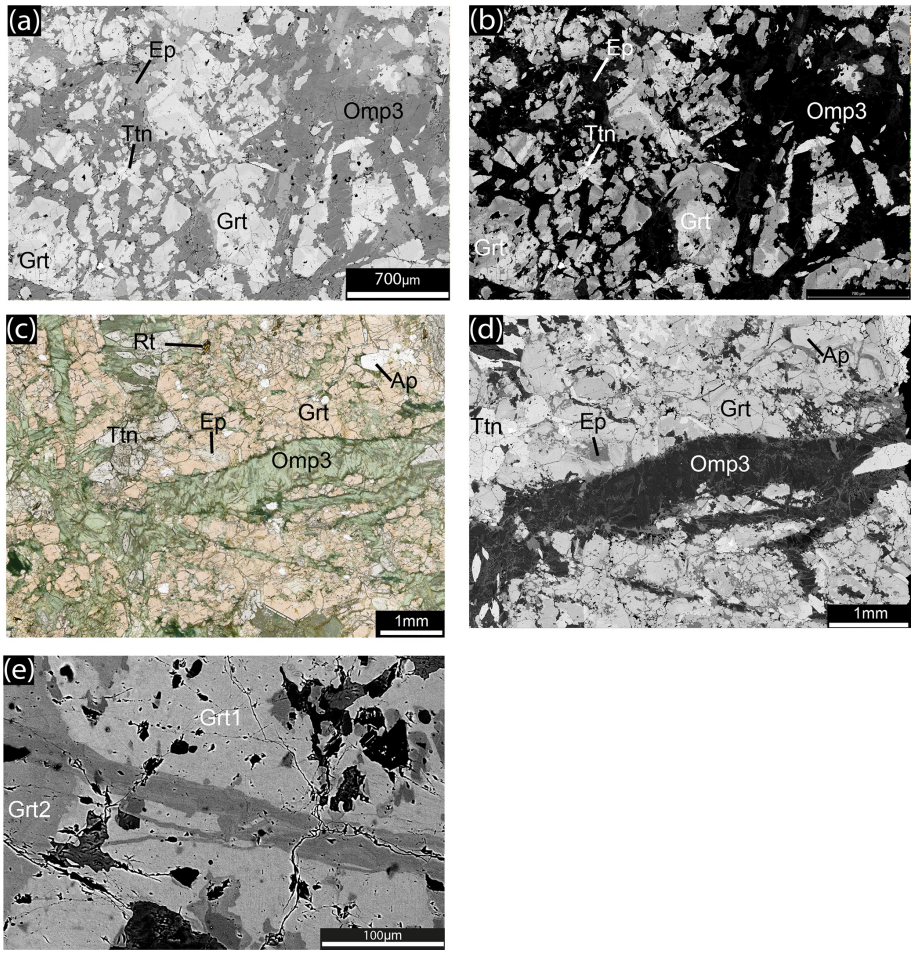

Figure 5. Microstructures of the Ca-metasomatite. **(a)** BSE image of garnet, titanite, and epidote fragments sealed by an Omp3 matrix. **(b)** BSE-enhanced contrast of the image **(a)** illustrating the fractured zoning pattern in the fragments of garnets. **(c)** Photomicrograph of a crack-seal vein of Omp3 cross-cutting the M2 assemblage. **(d)** BSE image of **(c)**. **(e)** BSE image showing a Grt1 cross-cut by a vein filled by Grt2. Abbreviations: Ttn, titanite; Ap, apatite (the other abbreviations are defined in the main text).

for the Ca-metasomatite, modeled at 2.5 GPa and 540 °C, the mass change is not associated with a significant volume strain ($\varepsilon = 0.91$) and can be considered isovolumetric. Mass change calculations indicate that the Ca-metasomatite displays a Ca mass gain of about 65 % and 375 % for P_2O_5 coupled with a loss of Na and Ti (67 %, 45 %) (Fig. 9b). For trace elements, the results indicate a mass gain of 1612 % for Sr and 2314 % for Cr (Fig. 9b).

Other major elements display an immobile behavior during metasomatism. It is worth noting that the mass change indicates a low mobility of Si between the unaltered rock and the Ca-metasomatite.

4.3 Thermodynamic modeling

4.3.1 Reference eclogite (the Sav2105 sample)

The pseudosection computed with the reference eclogite composition (Table 3) shows classical phase relations of an eclogite without hydrated minerals on the high-temperature side and an amphibole-bearing assemblage for 2.0 GPa $T \lesssim 580$ °C. Lawsonite is stable at 2.0 GPa/500 °C to 3.0 GPa/590 °C. The stability field of the eclogitic assemblage Grt1 + Omp1 + amphibole + rutile + lawsonite is between 515 and 555 °C and between 2.0 and 2.75 GPa (Fig. 10). Although no lawsonite was observed, it was likely present in the peak metamorphic assemblage, as evidenced by the presence of retrograde epidote, which is interpreted as a pseudomorph after lawsonite. The P–T conditions were refined using composition isopleths of garnet (Grt1) outermost rim and clinopyroxene (Omp1), at ∼ 2.5 GPa and ∼ 535 °C (Fig. 10).

4.3.2 Ca-metasomatite (Mez211002)

We performed thermodynamic calculations using the average bulk composition of reference eclogite to constrain the P–T conditions for the formation of the M2 assemblage,

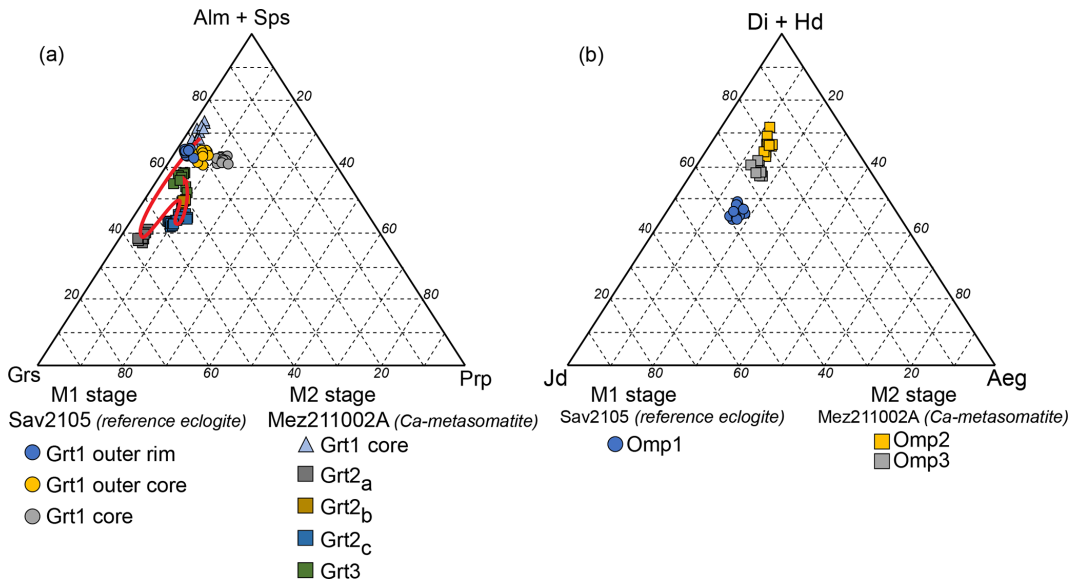

Figure 6. Ternary plot of different generations of garnet **(a)** and omphacite **(b)** from the M1 and M2 stages. The red arrow in **(a)** indicates the chemical evolution of the different Grt2 annuli.

which overgrows Grt1 and is thought to be related to Ca-metasomatism (Ca gain coupled with Na and K loss). To constrain P–T conditions and the effect of mass transfer on phase relations, P–X and T–X phase diagrams were computed, with X standing for the change in bulk composition. $X0$ corresponds to the mean reference eclogite bulk composition with a slight increase in Na_2O and a decrease in CaO. $X1$ is the mean Ca-metasomatite bulk composition with a 10 % increase in CaO and a 100 % loss of Na_2O. The chemical composition of the initial Ca-rich annulus in contact with Omp2 and surrounding the Grt1 core is used to constrain the P–T conditions. The chemical composition of omphacite inside atoll-shaped garnets or around garnets is the same (XJd 20 %–24 %, Fig. 7f). This uniform chemical composition is used as a thermo-barometer in P–X and T–X modeling. The Grt2 composition used for estimating the P–T conditions of the M2 stage is that of the first, Ca-rich, rim immediately surrounding either Grt1 or Omp2. The P–X pseudosection (Fig. 11a, b) is computed at a temperature of 535 °C, which corresponds to the temperature of the peak eclogitic conditions estimated in Sect. 4.3.1. The lawsonite stability field is not affected by the change in the bulk composition. The amphibole breakdown reaction occurred after $X = 0$ and 3.0 GPa to $X = 5$ and 1.8 GPa. In the T–X diagram, amphibole stability extends below $X = 0.2$ and at a temperature of 578 °C (Fig. 11). The increase in CaO in the system also has the effect of expanding the stability field of titanite to higher-P–T conditions together with rutile.

Rutile is destabilized between $X = 0.8$ and 1.8–500 °C and $X = 1$ and 3.0–630 °C. As shown in Fig. 11a, the same stability field of Cpx + Grt + Amp + Lws + Qtz + Rt is observed in the model for the reference eclogite. The compositional isopleths of Grt1 and Omp1 for the reference eclogite cross-cut each other and set the same conditions as in Fig. 10 with a pressure at 2.6–2.5 GPa. The isopleths of the first rim of Grt2 and Omp2 for the Ca-metasomatite intersect between 2.6 and 2.2 GPa (Fig. 11b). The crystallization conditions of the Ca-metasomatite assemblage fall within the lawsonite stability field (Fig. 11b). The T–X diagram was calculated at 2.5 GPa. Lawsonite is stable at temperatures lower than 580 °C. The isopleths of the M1 minerals, before the metasomatic event, are reported in Fig. 11b and d. For the M2 assemblage, the isopleths intersect in the same stability field of the P–X pseudosection (Fig. 11d), but they intersect in a temperature range of 578–505 °C. With the P–X and T–X diagrams, the P–T conditions of the M2 Ca-rich assemblages are estimated at 2.6–2.2 GPa and 578–505 °C. During the X variation and the CaO increase, the modal amount of lawsonite estimated is up to 8 vol % in P–T conditions of the metasomatism. The isopleths modeled for the first, Ca-rich, rim of Grt2 show an absolute error of 2 % for XAlm, 6 % for XGrs, and 3.5 % for XPrp with respect to the observed compositions. These deviations may result from (1) the use of an average bulk composition of unaltered eclogites that may not reflect the reactive bulk composition of the rock before Ca input and Na, K, and Ti leaching and (2) mineral assemblages and compositions, in the P–X and T–X models presented, being predicted at equilibrium, which may differ from natural systems (Lanari and Duesterhoeft, 2019).

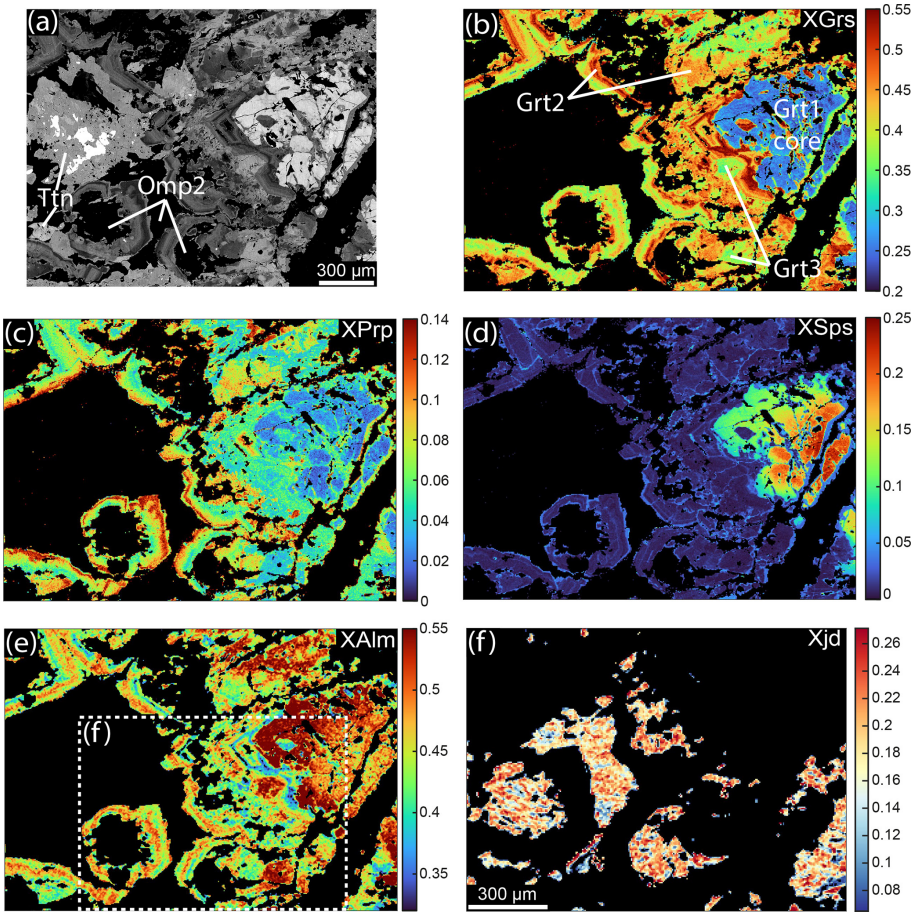

Figure 7. Garnet evolution of the M2 assemblage in the Mez211002 sample. **(a)** BSE-enhanced contrast image showing a Grt1 core surrounded by Grt2 with an oscillatory zoning pattern. The Grt2 also surrounds Omp2, giving the morphology of atoll garnet. **(b–e)** XAlm, XSps, XPrp, and XGrs standardized X-ray mapping. Note that the Grt1 appears with an enriched spessartine core and is cross-cut by a pyrope-rich garnet. The dotted white square in **(e)** is the location of **(f)**. **(f)** XJd standardized X-ray mapping of omphacite inside and around the Grt2.

5 Discussion

5.1 Reconstruction of the metamorphic and metasomatic history of metabasic rocks from the Savoney and Mezove units

Based on textural observations, chemical compositions, and P–T modeling, a succession of three metamorphic stages can be distinguished.

The petrological investigation of the unaltered eclogite sample (Sav2105) allows for the definition of the M1 stage peak metamorphic assemblage as Omp1 + Grt1 outer rim + glaucophane + rutile + lawsonite (Fig. 12a). There is no evidence of a reaction between the rock and an external fluid during the M1 stage. The phase diagram of the reference eclogite predicts a peak mineral assemblage of Cpx + Grt + Amp + Lws + Qtz + Rt. Quartz, with a modeled volume of up to 1 %, was not observed in the Sav2105 sample. The observed assemblage is Cpx + Grt + Amp + Lws + Rt, but the garnet and omphacite isopleths fit in the same field assemblage with quartz. The modeled peak P–T conditions for M1 are estimated at 2.5–2.6 GPa and 535 ± 40 °C and are consistent with other P–T estimates throughout the ZSZ (Bucher et al., 2005; Angiboust et al., 2009; Groppo et al., 2009; Angiboust and Agard, 2010; Bovay et al., 2022).

Relict Grt1 is also observed in the Ca-metasomatite, suggesting that both the reference eclogite from the Savoney unit and the mafic rocks in the Mezove unit shared a similar P–T history and initial bulk-rock composition before metasomatism. The M2 stage is interpreted as related to the percolation of an external Ca-rich fluid in the reference eclogite (Fig. 12b). During the ingression of the external fluid in the reference eclogite, the Grt1 core was partially to fully resorbed and the eventual relicts overgrown by the Ca-rich Grt2. The other phases Omp2, lawsonite (now epidote), apatite, rutile, and titanite grew coevally during this stage (Fig. 12). Thermodynamic modeling suggests that the M2 assemblage was stable at 2.6–2.2 GPa and 578–505 °C. The

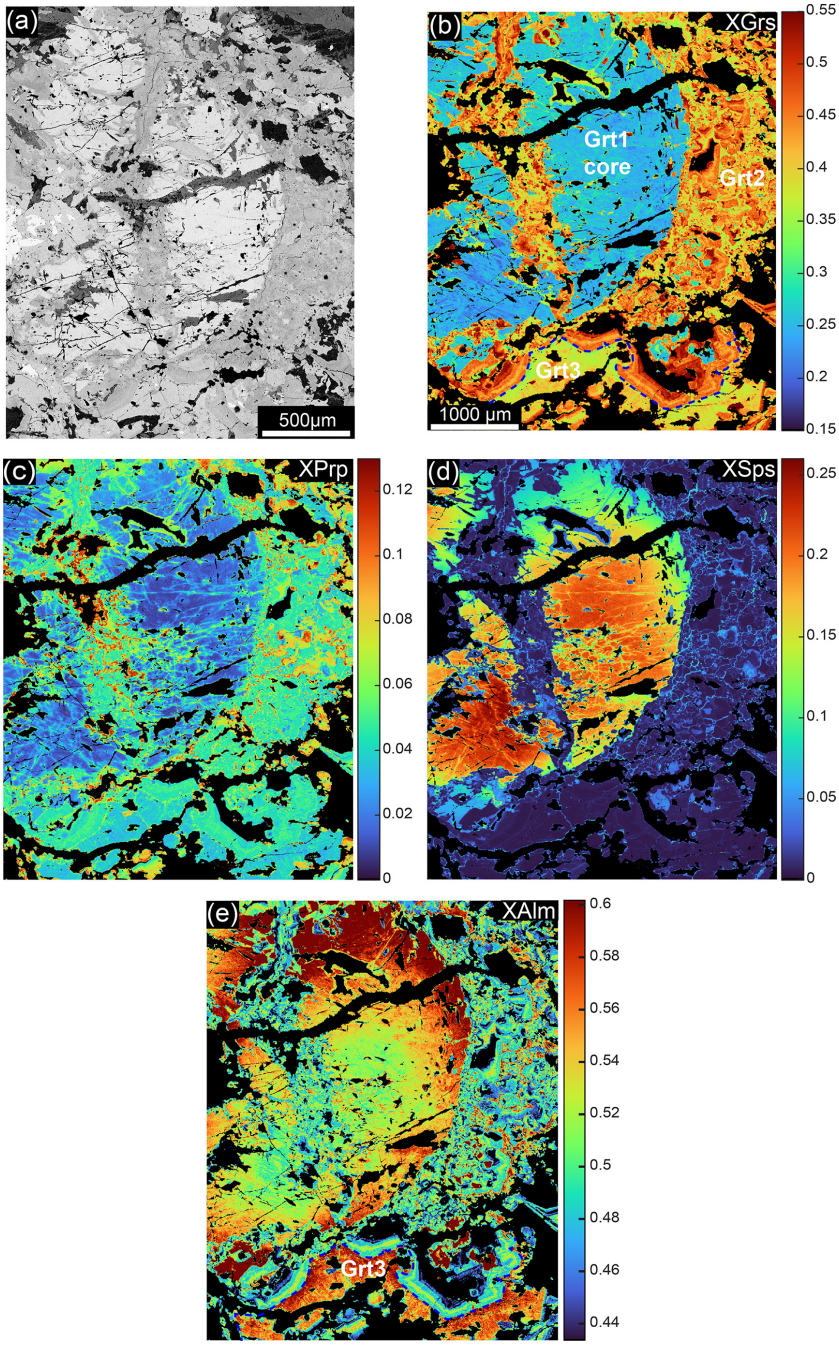

Figure 8. Garnet evolution from M1 to M2 assemblage in the Mez211002 sample. **(a)** BSE-enhanced contrast showing the brighter Grt1 core with dissolution embayment and the surrounding darker Grt2. **(b–e)** *X*Alm, *X*Sps, *X*Prp, and *X*Grs standardized X-ray mapping. Note that Grt1 appears with an enriched spessartine core and is cross-cut by fractures sealed by a pyrope-rich garnet. The fractures are visible on the *X*Prp and *X*Sps maps.

fluid–rock interaction and associated metasomatism could have occurred at any time between prograde burial and the onset of exhumation.

In the reference eclogite and the Ca-metasomatite, the K_2O content is below 500 µg g^{-1}, consistent with other measured mafic eclogite in the ZSZ (Barnicoat and Fry, 1986; Groppo et al., 2009; Angiboust and Agard, 2010; Weber and Bucher, 2015). The low bulk K content explains the absence of phengite in lawsonite pseudomorph products that contain instead Na-rich phases such as paragonite. In the Ca-metasomatite, only epidote was observed. The absence of paragonite suggests that the breakdown reaction of law-

Table 1. Major element composition of minerals from the M1 assemblage, extracted from the chemical map composition with XMapTools. Abbreviations: Tr, tremolite; Ftr, F-tremolite; Ts, tschermakite; Prg, pargasite.

Grt1	Core	Outer core	Outer rim	Omp1			Ep			Gln		
SiO_2	38.44	37.99	37.46	SiO_2	54.93	55.72	SiO_2	37.24	37.79	SiO_2	55.31	54.71
TiO_2	0.09	0.04	0.01	TiO_2	0.08	0.06	TiO_2	0.06	0.10	TiO_2	0.25	0.08
Al_2O_3	20.45	20.48	21.17	Al_2O_3	8.75	8.93	Al_2O_3	25.54	25.10	Al_2O_3	10.41	10.41
FeO	20.68	29.25	29.04	FeO	9.03	8.54	FeO	10.77	10.49	FeO	14.67	14.65
MnO	7.99	0.26	0.38	MnO	0.01	0.01	MnO	0.06	0.07	MnO	0.02	0.03
MgO	0.7	1.05	2.85	MgO	6.38	6.77	MgO	0.03	0.09	MgO	7.90	8.14
CaO	11.08	10.64	8.86	CaO	12.56	12.19	CaO	22.80	22.13	CaO	2.04	2.22
Na_2O	0.22	0.16	0.07	Na_2O	7.06	7.42	Na_2O	0.01	0.08	Na_2O	6.72	6.65
K_2O	0.02	0.02	0.02	K_2O	0.01	0.01	K_2O	0.02	0.01	K_2O	0.01	0.01
P_2O_5	0	0.01	0.01	P_2O_5	0.01	0.02	P_2O_5	0.02	0.02	P_2O_5	0.01	0.01
F	0	0	0	F	0.00	0.00	F	0.00	0.00	F	0.00	0.00
Cr_2O_3	0.07	0.06	0.09	Cr_2O_3	0.07	0.06	Cr_2O_3	0.05	0.05	Cr_2O_3	0.01	0.01
Total	99.81	100.02	100.01	Total	98.95	99.77	Total	96.59	95.92	Total	97.34	96.91
Si	3.05	3.02	2.96	Si	1.99	2.00	Si	2.95	3.00	Si	7.85	7.81
Ti	0	0	0	Ti	0.00	0.00	Ti	0.00	0.01	Al_iv	0.15	0.19
Al	1.91	1.92	1.97	Al	0.37	0.37	Al	2.38	2.35	Al_vi	1.59	1.56
Fe^{2+}	1.32	1.85	1.81	Fe^{2+}	0.14	0.11	Fe	0.71	0.70	Al_T2	0.15	0.19
Fe^{3+}	0.05	0.09	0.11	Fe^{3+}	0.12	0.14				Al_M2	1.59	1.56
Mn	0.54	0.01	0.02	Mn	0.00	0.00	Mn	0.00	0.00	Ti_M2	0.03	0.01
Mg	0.08	0.12	0.33	Mg	0.34	0.36	Mg	0.00	0.01	Fe_M2	0.20	0.22
Ca	0.94	0.9	0.75	Ca	0.48	0.46	Ca	1.94	1.90	Mg_M2	0.19	0.22
				Na	0.49	0.51				Fe_M13	1.54	1.53
*X*Alm	0.45	0.62	0.6	*X*Jd	0.36	0.37	*X*Ep	0.71	0.70	Mg_M13	1.48	1.52
*X*Prp	0.03	0.04	0.11	*X*Di	0.34	0.36	*X*Fep	0.00	0.00	Mn_M13	0.00	0.00
*X*Grs	0.32	0.3	0.25	*X*Hd	0.14	0.11	*X*Zo	0.28	0.30	Na_M4	1.69	1.66
*X*Sps	0.18	0.01	0.01	*X*Aeg	0.12	0.14	*X*Mep	0.00	0.00	Ca_M4	0.31	0.34
*X*And	0.02	0.03	0.03	*X*Mg	0.55	0.58				V_A	0.84	0.82
*X*Mg	0.05	0.06	0.15							Na_A	0.16	0.18
										*X*Mg	0.49	0.50
										*X*Fe	0.51	0.50
										*X*Gln	0.85	0.83
										*X*Tr	0.04	0.04
										*X*Ftr	0.04	0.04
										*X*Ts	−0.08	−0.08
										*X*Prg	0.16	0.18

sonite was not associated with Na-bearing phases such as glaucophane or omphacite (Lü et al., 2009) and that the amount of Na_2O available in the system was insufficient for the formation of paragonite. A similar process of lawsonite breakdown with epidote as the main product was reported in the Monte Emilius metabasites (Angiboust et al., 2017). The Ca-metasomatite shows a modal abundance of epidote of ∼ 10 %, contrasting the less than 5 % observed in the reference eclogite. Considering the amount of epidote to be a proxy for the amount of lawsonite present at the peak, this suggests that the Ca-metasomatite contained a significant amount of metasomatic lawsonite. However, Angiboust and Agard (2010) observed between 5 % and 10 % lawsonite pseudomorphs in metabasites from the ZSZ with classical MORB composition. Therefore, it is possible that the rock already contained a high-volume fraction of lawsonite prior to metasomatism. The mass balance analysis, however, shows a significant mass gain in both Ca and Sr. Considering that in peak conditions the main Sr-bearing phase is lawsonite (Martin et al., 2011; Lefeuvre et al., 2020), the mass gain should have resulted in an increase in the modal amount of lawsonite during metasomatism. This is consistent with other studies reporting the presence of metasomatic lawsonite in HP units (Martin et al., 2011; Angiboust et al., 2012b, 2017; Vitale-Brovarone et al., 2014; Piccoli et al., 2018).

The last Grt2 rim has a composition similar to that of a "closed"-system HP garnet but with slightly higher grossular and lower almandine proportions (Grt1 Alm_{61}–Grs_{30} vs. last Grt2 rim Alm_{50}–Grs_{38}), suggesting a possible re-equilibration in a closed system after the metasomatic stage.

Table 2. Major element composition of the minerals from the M2 stage, extracted from the chemical map composition with XMapTools.

	Grt1 core	Grt1 outer core	Grt2a	Grt2b	Grt2c	Grt2 last rim	Omp2			Ep2		
SiO_2	35.93	36.61	38.49	37.67	38.13	38.28	SiO_2	55.78	55.19	SiO_2	38.54	38.30
TiO_2	0.58	0.07	0.07	0.05	0.05	0.04	TiO_2	0.09	0.03	TiO_2	0.00	0.02
Al_2O_3	21.19	21.35	22.45	21.90	22.01	22.45	Al_2O_3	4.56	4.78	Al_2O_3	24.35	24.29
FeO	23.95	32.36	19.18	24.83	23.26	23.77	FeO	8.06	8.40	FeO	9.74	9.12
MnO	8.98	1.88	0.79	0.24	0.28	0.24	MnO	0.10	0.12	MnO	0.04	0.05
MgO	0.39	0.74	0.96	1.44	2.03	2.64	MgO	10.06	10.02	MgO	0.00	0.01
CaO	8.82	8.81	19.58	14.78	15.34	13.48	CaO	17.61	17.36	CaO	23.15	22.35
Na_2O	0.01	0.01	0.01	0.01	0.01	0.00	Na_2O	4.66	4.50	Na_2O	0.03	0.04
K_2O	0.02	0.02	0.05	0.05	0.01	0.02	K_2O	0.06	0.05	K_2O	0.07	0.07
P_2O_5	0.00	0.01	0.01	0.00	0.01	0.01	P_2O_5	0.02	0.01	P_2O_5	0.01	0.02
F	0.00	0.00	0.00	0.00	0.00	0.00	F	0.00	0.00	F	0.00	0.00
Cr_2O_3	0.02	0.02	0.02	0.02	0.02	0.02	Cr_2O_3	0.01	0.01	Cr_2O_3	0.02	0.02
Total	99.90	101.87	101.62	101.01	101.17	100.94	Total	101.01	100.47	Total	95.96	94.28
Si	2.90	2.90	2.95	2.94	2.95	2.96	Si	2.01	2.00	Si	3.06	3.09
Ti	0.04	0.00	0.00	0.00	0.00	0.00	Ti	0.00	0.00	Ti	0.00	0.00
Al	2.01	1.99	2.03	2.01	2.01	2.05	Al	0.19	0.20	Al	2.28	2.31
Mg	0.05	0.09	0.11	0.17	0.23	0.30	Mg	0.54	0.54	Mg	0.00	0.00
Fe^{2+}	1.48	1.94	1.16	1.50	1.41	1.49	Fe^{2+}	0.11	0.13	Fe	0.65	0.61
Fe^{3+}	0.13	0.21	0.07	0.12	0.09	0.05	Fe^{3+}	0.14	0.12	Mn	0.00	0.00
Mn	0.61	0.13	0.05	0.02	0.02	0.02	Mn	0.00	0.00	Ca	1.97	1.93
Ca	0.77	0.75	1.61	1.24	1.27	1.12	Ca	0.68	0.67	Al_M1	0.93	0.92
*X*Alm	0.49	0.62	0.39	0.50	0.47	0.50	Na	0.32	0.32	Al_M2	1.00	1.00
*X*Sps	0.20	0.04	0.02	0.01	0.01	0.01	*X*Mg	0.69	0.68	Fe_M1	0.00	0.00
*X*Prp	0.02	0.03	0.04	0.06	0.08	0.10	*X*Fe3	0.56	0.49	Al_M3	0.35	0.38
*X*Grs	0.25	0.24	0.54	0.41	0.42	0.38	Al_T1	0.01	0.01	Fe_M3	0.65	0.61
*X*And	0.04	0.07	0.02	0.04	0.03	0.02	Al_M1	0.18	0.19	Mn_M3	0.00	0.00
*X*Mg	0.03	0.04	0.09	0.10	0.14	0.17	SumM1	0.96	0.99	*X*Ep	0.65	0.61
							SumM2	1.00	0.99	*X*Fep	0.00	0.00
							*X*Jd	0.19	0.19	*X*Zo	0.35	0.38
							*X*Di	0.54	0.54	*X*Mep	0.00	0.00
							*X*Hd	0.11	0.13			
							*X*Aeg	0.14	0.12			

5.2 Garnet microstructures and zonation: evidence for external fluid infiltration

Petrographic observations reveal significant differences between the unaltered reference eclogite and the Ca-metasomatite. The variation in spessartine content across Grt1 follows a bell-shaped profile with a Mn depletion from core to rim. This chemical zonation is typical of a prograde growth of metamorphic garnet through a classical Rayleigh fractionation (Hollister, 1966; Atherton, 1968; Cygan and Lasaga, 1982; Evans, 2004).

Garnet grains with discontinuous and sharp compositional zoning are often ascribed to polycyclic metamorphic evolution in the Alps, e.g., the Sesia zone (Konrad-Schmolke et al., 2006; Engi et al., 2018; Giuntoli et al., 2018a, b; Vho et al., 2020), continental allochthons in the ZSZ (Angiboust et al., 2017; Hertgen et al., 2017), the Dent Blanche unit (Manzotti et al., 2012), the Dora-Maira unit (Gasco et al., 2011; Nosenzo et al., 2023), the Gran Paradiso unit (Manzotti and Ballèvre, 2013; Manzotti et al., 2024), Alpine Corsica (Martin et al., 2011), the central Alps (Thöni and Miller, 2009; Herwartz et al., 2011; Sandmann et al., 2014), or in other collision belts (Feenstra et al., 2007; Fazio et al., 2009; Brandt and Schenk, 2020). Similar discontinuous compositional zoning in garnets was described in mono-metamorphic terranes in the Alps (Konrad-Schmolke et al., 2008; Angiboust et al., 2011, 2012b, 2014a; Rubatto and Angiboust, 2015; Locatelli et al., 2018; Broadwell et al., 2019; Bovay et al., 2022). Oscillatory concentric zonation in the garnet rim is reported, in some cases, during discontinuous garnet growth (Kulhánek and Faryad, 2023). The processes invoked for the formation of discontinuous compositional zoning and related oscillatory zoning are compatible with closed and open systems. In a closed-system growth, concentric-ring or

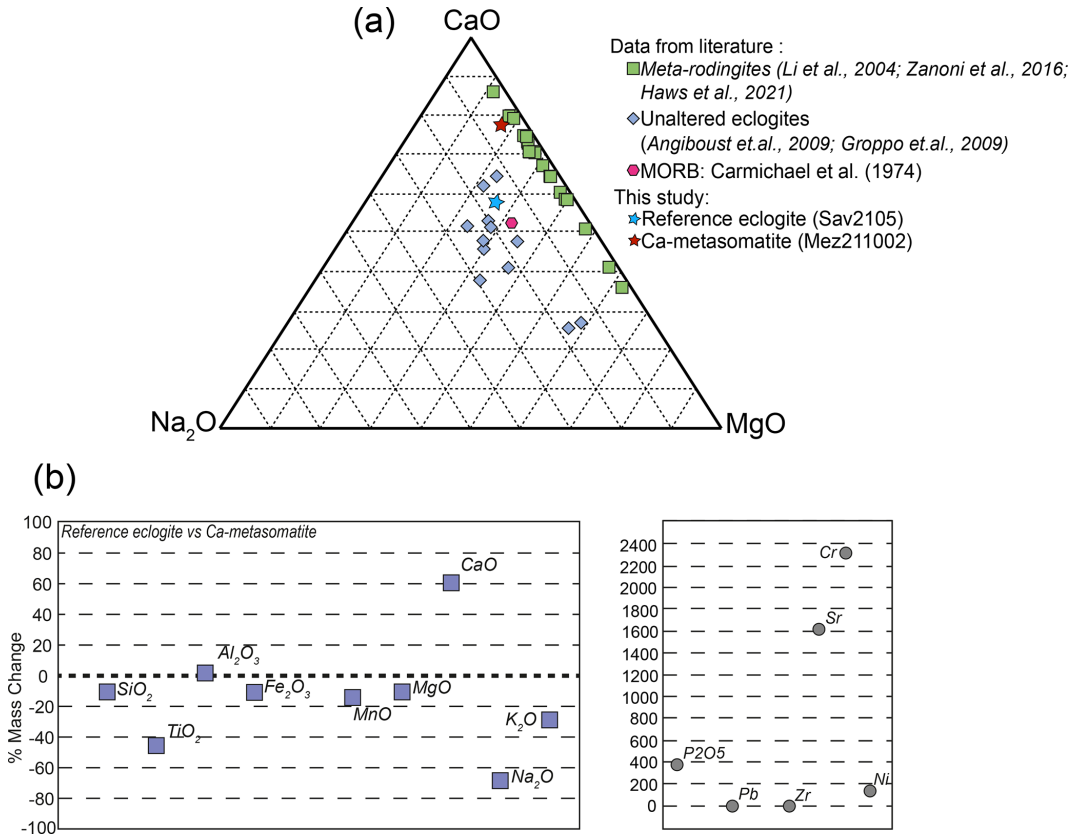

Figure 9. **(a)** Ternary plot in the system CaO–MgO–Na_2O of unaltered eclogite from the Zermatt-Saas zone (Groppo et al., 2009; Angiboust and Agard, 2010; this study), metarodingite (Li et al., 2004; Zanoni et al., 2016; Haws et al., 2021), and Ca-metasomatite (this study). **(b)** Mass change in percentage for major and selected trace elements for the Ca-metasomatite compared with the reference eclogite. Zirconium is used as an immobile species.

Table 3. Bulk-rock compositions used for mass balance calculation and in Perple_X. LOI denotes loss of ignition.

Samples/elements (wt %)	SiO_2	TiO_2	Al_2O_3	Fe_2O_3(T)	MnO	MgO	CaO	Na_2O	K_2O	P_2O_5	LOI
Mez211002(A)	40.72	2.9	14.7	17.14	0.36	4.09	18.53	1.02	0.02	0.81	0.37
Mez211002(B)	41.68	2.83	14.01	16.31	0.34	4.39	18.1	1.44	0.02	0.72	0.38
Mez220801	42.06	2.4	13.83	16.25	0.32	4.68	17.76	1.71	0.00	0.71	0.50
Mez211003	39.03	6.18	14.67	17.35	0.39	3.60	17.83	0.94	0.05	0.33	0.06
Mean	40.87	3.57	14.30	16.76	0.35	4.19	18.05	1.27	0.02	0.64	0.32
Sav0601	44.28	6.13	12.82	17.54	0.38	4.88	10.55	3.84	0.05	0.13	0.03
Sav2105	39.84	5.82	11.99	17.49	0.38	5.62	12.41	3.24	0.01	0.11	3.51
Sav2105 (pondered effective bulk)	43.61	6.37	13.12	18.27	0.41	4.20	10.32	3.55	0.02	0.12	0.00
Mean bulk (Sav0601, eff. bulk Sav2105)	43.95	6.25	12.97	17.91	0.40	4.54	9.03	4.05	0.04	0.13	1.77
Bulk Perple_X (wt %)	**SiO_2**	**TiO_2**	**Al_2O_3**	**FeO**	**Fe^{3+}**	**MgO**	**CaO**	**Na_2O**	**K_2O**	**P_2O_5**	
Eff. bulk Sav2105	43.61	6.37	13.12	13.63	2.79	4.20	10.32	3.55	0.00	0.00	
Mean reference eclogite	43.95	6.25	12.97	13.21	2.89	4.54	9.30	4.05	0.00	0.00	
Mean Ca-metasomatite bulk	40.87	3.58	14.30	15.08	4.37	4.19	22.3	0.00	0.00	0.00	

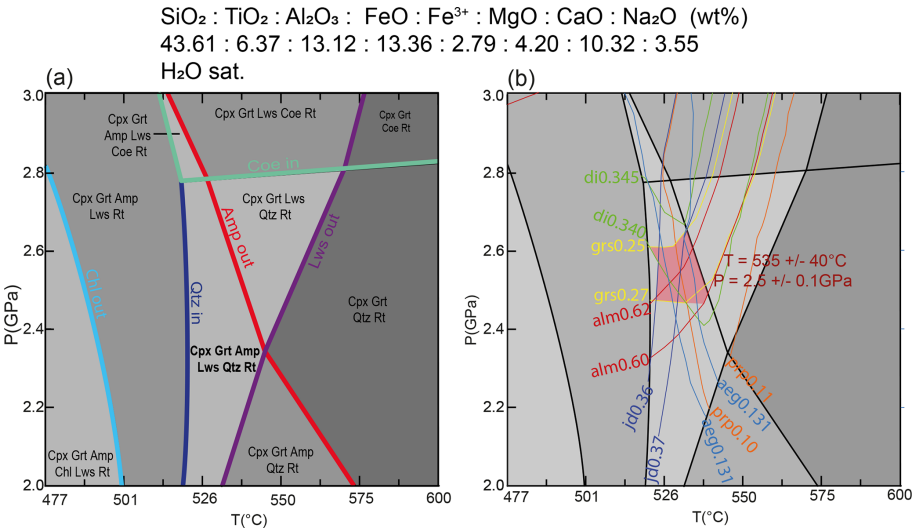

Figure 10. Pseudosection modeled in NCFMASHTi using Perple_X. The effective bulk composition of the Sav2105 sample is given in Table 3. Abbreviations: Cpx, clinopyroxene; Grt, garnet; Amp, amphibole; Lws, lawsonite; Rt, rutile; Coe, coesite; Qtz, quartz; Chl, chlorite.

sharp chemical zonation results from the availability of garnet nutrient partitioned during the breakdown of element-rich source minerals such as chlorite, lawsonite, epidote, or amphibole (Pyle and Spear, 1999; Yang and Pattison, 2006; Raimondo et al., 2017; Hyppolito et al., 2019; Rubatto et al., 2020; Gaidies et al., 2021) and/or a complex interplay between the growth rate of the crystal and the availability, solubility, and intergranular mobility of elements (Konrad-Schmolke et al., 2005, 2008). For the open-system scenario, the oscillatory chemical zoning was suggested to form after infiltration of an external fluid out of equilibrium with the system, sometimes during pulsed fluid influx (Dziggel et al., 2009; Angiboust et al., 2012a, 2014a; Moore et al., 2013; Giuntoli et al., 2018a; Hyppolito et al., 2019; Locatelli et al., 2019; Vho et al., 2020; Bovay et al., 2022) and/or during external fluid fractionation (Rubatto and Angiboust, 2015).

The P–T conditions of the M2 stage suggest that chlorite breakdown occurred along the prograde path, whereas amphibole breakdown occurred at the onset of the metasomatism. Even if these two hydrated minerals released fluids into the system, they cannot be responsible for the addition of CaO during the M2 stage. Furthermore, under these P–T conditions, there is no evidence of a breakdown of Ca-bearing phases in the reference eclogite (e.g., lawsonite, epidote, and apatite) that could internally leach the Ca necessary for the crystallization of the Grt2 and an increase in modal abundance of lawsonite in the M2 stage. Moreover, the redistribution of CaO, in this case, does not reflect the mass gain in the Ca-metasomatite. Therefore, CaO must have been transported into the system by an external fluid. This is supported by Grt1 textures in the M2 assemblage, displaying lobate edges, peninsulas, and embayments indicative of relict garnet porphyroblasts having experienced dissolution during interaction with an external fluid out of equilibrium with the system. The annular and oscillatory chemical zoning of Grt2 also supports the argument for an external fluid-driven crystallization during a pulsed influx of external Ca-rich fluids, rather than crystallization in a closed system. These fluid pulses transported CaO and leached out Na_2O and K_2O, resulting in the growth of Ca-rich annuli followed by a return to equilibrium, as indicated by the growth of Fe-rich–Ca-poor rings.

5.3 Ca-rich fluid–rock interaction or rodingitization?

Rodingitization occurs at mid-oceanic ridges (Li et al., 2004, 2008; Panseri et al., 2008; Zanoni et al., 2016; Laborda-López et al., 2018) or in subduction environments (Li et al., 2008; Tsikouras et al., 2009; Dai et al., 2016) and is defined by a reaction of an external Ca-rich and Si-poor fluid with mafic rocks (Coleman, 1967; Frost, 1975; Schandl et al., 1990; O'Hanley et al., 1992). This Ca-rich metasomatism results in bulk-rock metasomatism involving enrichment in CaO; depletion in Na_2O and SiO_2; and the formation of a typical mineral assemblage consisting of hydrogrossular garnet, diopside, clinozoisite, epidote, and vesuvianite. This mineral assemblage is stable over a wide range of P–T conditions, and determining whether it occurred during oceanic alteration or subduction metamorphism requires a careful evaluation.

The analyzed samples (Mez211002 and Sav2105) are plotted along with metamorphic rodingite (metarodingite; Haws et al., 2021) and eclogite compositions of the ZSZ (Groppo et al., 2009; Angiboust and Agard, 2010) on a CaO–Na_2O–MgO ternary diagram (Fig. 9a). The bulk-rock composition of the reference eclogite is similar to that of the eclogitic metabasites of the ZSZ (see Sect. 4.2). The elevated Fe and

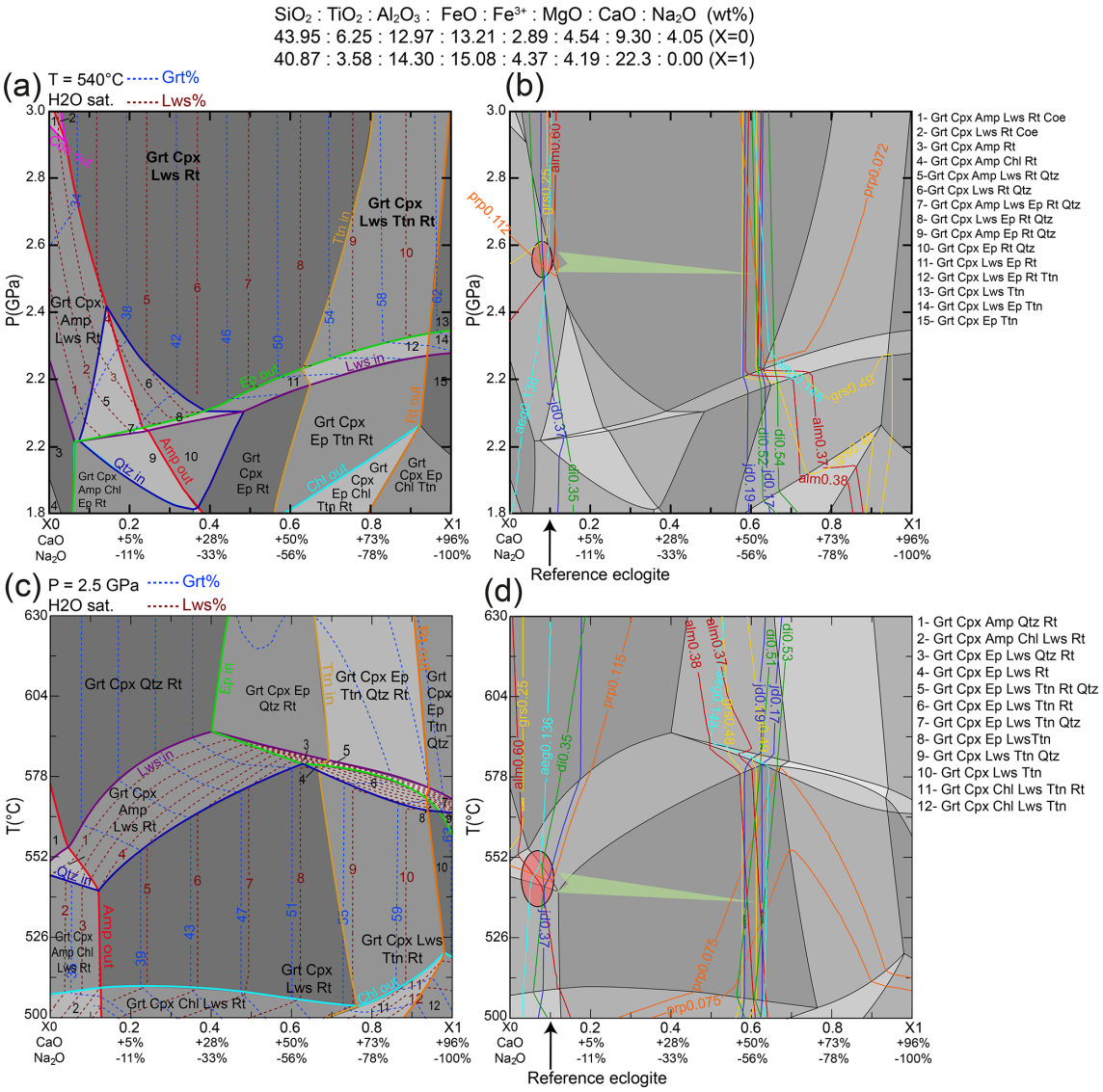

Figure 11. **(a)** P–X compositions calculated at $T = 540\,°C$ under water-saturated conditions and in the NCFMASHTi system. The x axis is the variation in the bulk composition ranging from $X0$, the mean bulk composition of reference eclogite (Table 3), to $X1$, the mean Ca-metasomatite with a 96 % gain of CaO and a 100 % loss of Na_2O. **(b)** P–X pseudosection identical to **(a)** showing only the model chemical isopleths of garnet and omphacite. **(c)** T–X composition calculated at $P = 2.5$ GPa in the same conditions and with the same previous x axis. **(d)** T–X identical to **(c)** showing only the model chemical isopleths of garnet and omphacite.

Ti contents observed in both the reference eclogite and Ca-metasomatite samples indicate that the composition is more akin to that of a Fe–Ti gabbro than a metabasalt.

In the ternary plot of Fig. 9a, the Ca-metasomatite falls close to the Ca-rich metarodingites from the Western Alps and the Voltri Massif but with a higher Na_2O content (Li et al., 2008; Zanoni et al., 2016; Haws et al., 2021). The higher Na_2O content in the Mez211002 sample is consistent with the high jadeite fraction observed in Omp2 ($Jd_{17–19}$) and the late-stage Omp3 ($Jd_{26–28}$). Clinopyroxene in oceanic metarodingite is usually Ca–Mg diopside, and Na-clinopyroxene (e.g., omphacite) has never been described. The second major difference between the studied Ca-metasomatite and other metarodingites is that the mass balance analysis shows no silica depletion in the bulk-rock composition.

Altogether, these characteristics suggest that the Ca-metasomatism described here differs from the classical rodingitization reaction, and therefore the samples studied do not represent an oceanic rodingite that equilibrated during subduction metamorphism (Frost and Beard, 2007; Li et al., 2008; Bach and Klein, 2009; Laborda-López et al., 2018).

The metasomatic process characterized here has striking analogies with other examples of high-pressure Ca-metasomatism reported in the Alpine orogen, where the

metasomatic event leads to crystallization and an increase in the modal quantity of classical HP minerals such as garnet, clinopyroxene, and lawsonite, sometimes associated with carbonates (Angiboust et al., 2011; Martin et al., 2011; Vitale-Brovarone et al., 2014; Piccoli et al., 2016, 2018; Angiboust et al., 2017; Hertgen et al., 2017; Weber et al., 2022). From these analogies, we propose that the Ca-metasomatism affecting the Mez211002 sample results from an interaction, during subduction, between a Ca-rich aqueous fluid and a formerly eclogitized Fe–Ti gabbro with a garnet, omphacite, rutile, and lawsonite (now epidote) assemblage. Furthermore, the unaltered SiO_2 content in the rock results in the crystallization of a mineral assemblage similar to that of eclogitic Fe–Ti metagabbros, enriched in Ca and depleted in Na_2O and TiO_2, rather than a typical assemblage of rodingite. However, ocean floor metasomatism could also have locally affected the oceanic crust before the subduction.

5.4 Origin and composition of metasomatizing fluids

Numerous examples of Ca-metasomatism have been reported worldwide (Beinlich et al., 2010; Vitale Brovarone and Beyssac, 2014; Piccoli et al., 2016; Angiboust et al., 2017; Hertgen et al., 2017; Li et al., 2017; Piccoli et al., 2018) and often suggest that Ca derives from metasedimentary rocks such as calc-schists and marbles from nearby units. In these studies, the leaching of CaO is associated with decarbonation or carbonate dissolution and the subsequent formation of CO_2- or CH_4-rich fluids (Ague and Nicolescu, 2014; Vitale-Brovarone et al., 2017; Menzel et al., 2020). The unaltered reference eclogite contains a small amount of dolomite in the matrix. However, the absence of carbonate minerals in inclusions in the relict Grt1 in both the reference eclogite and the Ca-metasomatite sample suggests that the rock did not originally contain carbonate. Moreover, the absence of metasomatic carbonate, e.g., formed by carbonation reaction during metasomatism, suggests that the metasomatizing fluid had a very low CO_2 content before entering the system or that the CO_2 did not react with the host rock during metasomatism. This observation indicates that the metasomatizing fluid is unlikely to be derived solely from metasedimentary rocks, since such a fluid would be expected to have high X_{CO_2} and a characteristic trace element signature, with enrichment in, for example, Rb, Ba, Cs, and Pb (Zack and John, 2007; Hermann and Rubatto, 2009). Trace element mass balance analysis shows significant enrichments in Sr and Cr. Strontium is enriched not only in metasedimentary rocks but also in metabasite, where the dehydration of Ca-bearing phases such as lawsonite and epidote can release a significant amount of Sr into the fluid (Halama et al., 2011; Martin et al., 2011, 2014; Herms et al., 2012; Gilio et al., 2020). The Cr enrichment is more difficult to explain as its concentration in the metasomatic garnet and omphacite is comparable to that measured in the unaltered samples. In addition, the small number of samples makes a statistical approach difficult. In other studies, metasomatic Cr enrichment in the bulk-rock composition is generally associated with Cr-rich oscillatory zoning in metasomatic garnet, omphacite, or lawsonite and is often interpreted to reflect the pulsed infiltration of fluids with mafic or ultramafic signatures (Tsujimori et al., 2006; Angiboust et al., 2011, 2014a; Spandler et al., 2011; Vitale-Brovarone et al., 2014; Piccoli et al., 2018; Locatelli et al., 2019). In the absence of this microtextural feature, it is not possible to conclude definitively whether the Cr enrichment is associated with fluid infiltration and is not due to initial local bulk composition variability.

In the study area, large numbers of ultramafic rocks are exposed in the Mont Avic ultramafic unit (Fig. 1c), and the Ca-metasomatite blocks are surrounded by serpentinites. Serpentinites are a major fluid source in the subducted (ultra)slow oceanic lithosphere (Schmidt and Poli, 1998, 2013; Rüpke et al., 2004). Major dehydration reactions in serpentinites are the brucite-out reaction occurring at 500 °C and 1.5–2.0 GPa (brucite + antigorite → olivine + H_2O; Scambelluri et al., 1991; Ulmer and Trommsdorff, 1999; Padrón-Navarta et al., 2010; Kempf et al., 2020) and the antigorite-out reaction occurring at 640–520 °C and ∼ 2–5 GPa (antigorite → forsterite + enstatite + chlorite + H_2O; Ulmer and Trommsdorff, 1999; Bretscher et al., 2018). In the locality studied, the brucite-out reaction is consistent with the observation of olivine + Ti-clinohumite veins in the Mont Avic ultramafic unit (Fontana et al., 2008). It is therefore possible that the Cr enrichment in the Ca-metasomatite is due to the infiltration of a fluid generated by the breakdown of brucite. Alternatively, deep serpentinization and prograde replacement of clinopyroxene by antigorite at depth could also be a potential source of Ca and Cr (Hyndman and Peacock, 2003; Deschamps et al., 2013; Vitale-Brovarone et al., 2017). The enrichment in Sr correlated with Cr could indicate a fluid source from Al–Mg metagabbros (Locatelli et al., 2019).

Altogether, considering the lack of mineral carbonation; the bulk enrichment in Ca, Sr, and Cr; and the petrological and geochemical analogies with other HP metasomatic rocks worldwide, we suggest that the metasomatizing fluid had a mixed source and its composition resulted from the interaction with calc-schist or marble, Al–Mg metagabbro, and nearby or mantle-derived ultramafic rocks (Martin et al., 2011; Spandler et al., 2011; Angiboust et al., 2012b, 2014; Vitale-Brovarone et al., 2014; Rubatto and Angiboust, 2015; Piccoli et al., 2016; Locatelli et al., 2019; Muñoz-Montecinos et al., 2021).

5.5 Fluid fluxes and metasomatism of eclogitic blocks during subduction

Studies focusing on fluid fluxes in subduction zones report a large range of estimates, from near zero to more than $10^3\ m^3_{fluid}\ m^{-2}_{rock}$. Here we use the results of the mass balance calculation to estimate the time-integrated fluid flux required to achieve metasomatism and thus to determine whether the

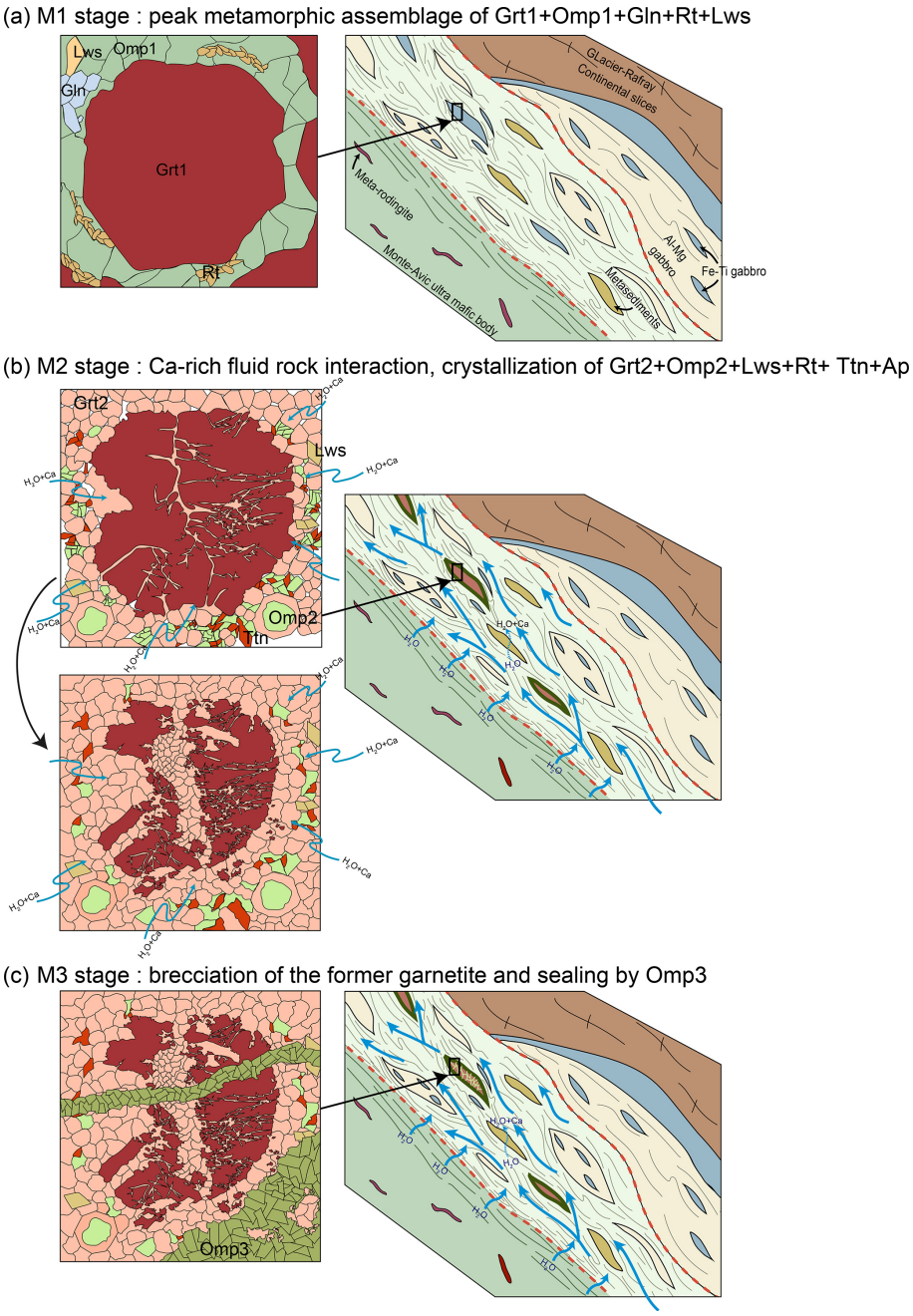

Figure 12. Representative sketch illustrating the sequence of metamorphic stages. For each stage, the thin-section-scale sketch is associated with a larger-scale sketch representing the shear zone in a subduction setting position. The eclogitic assemblage from the reference eclogite (M1) undergoes replacement, either partial or total, by the Ca-rich mineral assemblage (M2) as a consequence of channelization of Ca-rich external fluid along the shear zone. During the M2 stage, relicts of Grt1 core are surrounded by Grt2. Lastly, the M2-stage-related garnetite-like rock is brecciated and fragments of Grt2 are sealed by the Omp3 matrix.

system behaves in an open or closed manner (Oliver, 1996; Ferry and Gerdes, 1998). Computation of the time-integrated fluid flux in an advection-dominated system can be simplified using the equation of Ague (2013):

$$q_{\mathrm{TI}} \approx L_{\mathrm{GF}} \frac{n_i}{C_i^{\mathrm{eq}} - C_{i,x=0}^{\mathrm{input}}},$$

where L_{GF} is the length of the geochemical front, n_i the number of moles of i (here CaO) produced or consumed per unit volume rock (m^3), $C_{i,x=0}^{\mathrm{input}}$ the concentration of element i in the external reacting fluid, and C_i^{eq} the mass fraction of element i after re-equilibration in the system. For the calculation, L_{GF} corresponds to the length of the outcrop, about

100 m in the present case. For a conservative estimation of the fluid fluxes, it can be assumed that all Ca of the fluid is transferred to the rock during the reaction, so C_i^{eq} is set to 0. The number of moles of CaO produced during the reaction, n_{CaO}, is derived from the mass balance calculations (Fig. 9b). It corresponds to a mass gain of 65 % (∼ 6.65 wt %), that is, 1.19 mol kg^{-1}. Using a density of the Ca-metasomatite of 3673 kg m^{-3} (modeled at 2.5 GPa and 540 °C), the absolute mass gain corresponds to 4340 mol m^{-3}. Two different Ca molality values can be found in the literature. The first value is about 0.3 mol kg^{-1} H_2O (Connolly and Galvez, 2018). This molality is derived by the calculation assuming dehydration of a metasedimentary rock with a GLOSS composition (i.e., global subducted sediments; Plank and Langmuir, 1998). In this study, we can use this value to model a fluid derived solely from the adjacent metasediments. In addition, since this value is the largest of the two values found in the literature, the computation should provide an estimation of the minimum value of the fluid flux. The second Ca molality value available in the literature is ∼ 8×10^{-3} mol kg^{-1} H_2O (Manning, 2004). This molality value corresponds to that of a fluid equilibrated with a metabasite with N-MORB composition (John and Schenk, 2003; Zack and John, 2007). The fluid is therefore assumed to have the same composition as that of a fluid expelled by metabasite dehydration (Beinlich et al., 2010). Considering that in our study area the metasomatic lens is surrounded by serpentinites, it can be hypothesized that the fluid liberated from the serpentinites equilibrated with the mafic lenses during flow. In the first scenario (unique sediment source), the time-integrated fluid flux is 1.21×10^3 m^3 m^{-2}, while in the second scenario (fluid derived from metabasite dehydration), the value is 4.52×10^4 m^3 m^{-2} (Fig. 13, Table S2).

Figure 13 summarizes the results of the time-integrated fluid flux computation for various geodynamic settings. Plotting the range of values between our minimum (metasediments as the fluid source) and maximum (serpentinites as the fluid source) estimates obtained above in Fig. 13 shows that, whatever the source, the estimated values require a channelized flow, suggesting an open-system behavior. Moreover, a pervasive fluid flow would be too slow to allow both the resorption of Grt1 and the crystallization of Grt2 (Giuntoli et al., 2018a). The time-integrated fluid flux values can be compared with estimates from other Alpine HP metamorphic domains. In the ZSZ Theodul Glacier unit, Bovay et al. (2021) derive a 1.1×10^3 m^3 m^{-2} value, which is close to the lower estimation obtained here (1.3×10^3 m^3 m^{-2}). Fluid flux estimates derived for the HP metamorphic rocks of the Sesia zone, more specifically from mafic boudins, are between 1.7×10^3 and 2.2×10^3 m^3 m^{-2} (Vho et al., 2020). This range of values is also in agreement with our results.

Considering the local geology, the volume of metasedimentary rocks and serpentinites needed to produce the obtained fluid fluxes can be back-calculated (Table S2). Metasediments have a density of 2600 kg m^{-3} (Connolly and Galvez, 2018), and the water content released at 2.5 GPa and 550 °C is about ∼ 2 wt % (Kerrick and Connelly, 2001), with a density of 1200 kg m^{-3}. In the first case, 3.04×10^4 m^3 of dehydrated sediments is required to produce the estimated fluid fluxes. In the second case, where serpentinites are the main fluid source, the amount of fluid released from the brucite-out reaction is ∼ 3 wt % (Padrón-Navarta et al., 2010). Serpentinites have a similar density to metasediments. In this case, 7.60×10^5 m^3 of serpentinites is necessary to produce the estimated fluid fluxes. Metasediments from the nearby Saint-Marcel (Tartarotti et al., 2017b) and Champorcher-Miserin units (Tartarotti et al., 2017c, 2019; Rotondo et al., 2021; Scambelluri et al., 2022) or serpentinites from the Mont Avic ultramafic unit (Fontana et al., 2008, 2015) are possible units of sufficient volume to provide a suitable amount of fluid for the metasomatic reaction. Furthermore, sediment slices embedded in the serpentinite matrix of the Mezove unit (Angiboust et al., 2009; Angiboust and Agard, 2010) could contribute as a Ca source to a serpentinite-derived fluid. However, further studies are required to verify this hypothesis.

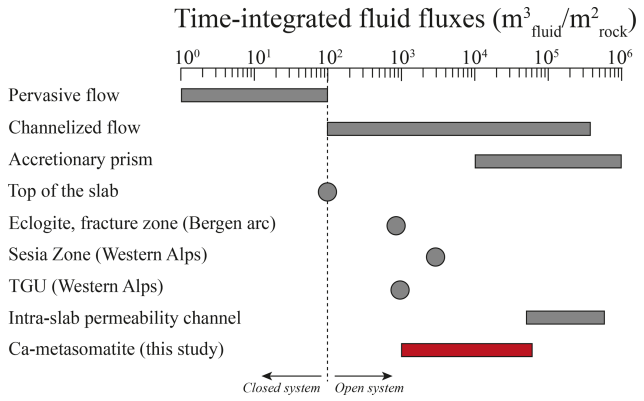

Figure 13. Time-integrated fluid flux for various geodynamic systems (modified after Piccoli et al., 2021, and Zack and John, 2007). Data are taken from the following sources: pervasive and channelized flows in subduction zones from Cannat et al. (2010) and Van Keken et al. (2011), accretionary prism from Ague (2013), top of the slab from Zack and John (2007), Sesia zone from Vho et al. (2020), TGU from Bovay et al. (2021), and intra-slab high-permeability channels from Piccoli et al. (2021).

5.6 Rheological implication of the brecciation M3 stage

The last M3 stage corresponds to the brecciation of the M2 assemblages and the crystallization of Omp3 in the matrix (Fig. 12c). Oscillatory zoning in garnet has been proposed to be the record of fluid pulses associated with cyclic seismic events (Angiboust et al., 2012a, 2014a; Viete et al., 2018; Hoover et al., 2022). In some cases, zonation in garnet is also associated with brecciation textures, suggesting that fluid flow is favored by multiple rupture events (Lo-

catelli et al., 2018). In our study, metasomatic Grt2 generation displays oscillatory zoning, indicating pulsed fluid influxes. A prominent feature of the Ca-metasomatites from the Mezove shear zone is that HP metasomatism is followed by intense brecciation. In the Monviso ophiolitic complex, eclogitic breccias were described along shear zones and are localized in more resistant Fe–Ti metagabbros embedded in Al–Mg metagabbros. The development of these brittle events is attributed to a combination of rheological contrast between the Fe–Ti and Al–Mg metagabbros, along with variations in the strain rate and/or pore fluid pressure (Angiboust et al., 2011, 2012a; Locatelli et al., 2018, 2019; Broadwell et al., 2019). For the Mezove shear zone, the brecciation event followed the metasomatism and the formation of the Ca-metasomatite at the expense of the Fe–Ti block. The mosaic breccia texture, exhibiting no displacement during brittle deformation, could be the result of increasing pore pressure during fluid influx. The fluid flux leading to brecciation is evidenced by the occurrence of hydrated phases, like lawsonite pseudomorph (now epidote), albeit in lesser abundance, within the matrix, which is similar to observations in the Monviso breccia matrix (Angiboust et al., 2011, 2012a; Locatelli et al., 2018, 2019). Both numerical and experimental investigations have demonstrated that an increasing garnet content enhances the strength of eclogite and promotes the transition from predominantly crystal plastic to brittle-dominated deformation (Rogowitz et al., 2023). This transition typically occurs under low strain rates, below seismic strain rates of $1\,s^{-1}$ (Yamato et al., 2019). Regarding the Ca-metasomatized block, we propose that the brecciation event could be the effect of an increase in garnet content during the M2 metasomatic stage, leading to a strong rheological contrast between the Ca-metasomatized block and the serpentinite matrix, thereby facilitating strain localization. Additionally, the brecciation may have been facilitated by an increase in internal pore pressure. The question remains as to whether the fluids caused an increase in internal pore pressure, triggering brittle deformation (e.g., by decreasing the normal stress acting on potential rupture surfaces), or whether brittle deformation is responsible for the fluid migration and arrival in the system by increasing permeability.

6 Conclusions

Petrological, geochemical, and microstructural studies of HP metasomatic rocks are essential to better understand the processes that regulate fluid flow in subduction environments. In this study, we show that the rocks found along a shear zone separating mafic rocks from the ultramafic oceanic lithosphere were intensely metasomatized and that fluid flow was accompanied by brittle deformation.

Petrological and geochemical features indicate that the metasomatizing aqueous fluid was Ca-rich and that metasomatism occurred in HP conditions, triggering the recrystallization of the original eclogite assemblage into a Ca-rich metasomatic assemblage. The Ca–Fe oscillatory zoning in the metasomatic garnet indicates pulsed fluid infiltration events interrupted by a period of re-equilibration. Open-system thermodynamic modeling constrains the Ca-rich metasomatism under eclogitic conditions between 2.2–2.6 GPa and 500–550 °C, during prograde to peak or early retrograde metamorphism. These P–T conditions suggest two possible dehydration reactions for the fluid sources: (1) the partial dehydration of the underlying serpentinites via the brucite-out reaction along the prograde path or (2) the breakdown of lawsonite in the mafic lithologies during exhumation. Given the Ca, Sr, and possible slight Cr enrichment, plausible fluid sources could be the dehydration of slab serpentinites, metabasites, and metasediments and also deep serpentinization and associated Ca release.

This conclusion is supported by the high time-integrated fluid fluxes (1.21×10^3 to $4.52 \times 10^4\,m^3\,m^{-2}$), which can be achieved considering the volume of serpentinites underlying the metasomatized contact. However, the mass balance analysis also shows prominent Ca and Sr enrichment, suggesting that the fluid composition evolved during the reactive fluid flow. Lastly, brecciation textures with an omphacite-supported matrix may have resulted from the increased garnet content and the associated change in rheological contrast between the Ca-metasomatite block and the weaker serpentinite matrix as well as an increase in internal pore pressure that could have helped brittle deformation to proceed at a lower strain rate than in classic eclogite.

Data availability. Data in the three tables are original data obtained by the authors. The other data used in Figs. 9a and 13 are from the literature. The data set required for the reproduction of these tables and figures can be accessed at the following link: https://doi.org/10.25666/DATAUBFC-2024-07-18 (Lecacheur et al., 2024).

Supplement. The supplement related to this article is available online at: https://doi.org/10.5194/ejm-36-767-2024-supplement.

Author contributions. This study was completed by KL as part of their PhD research supervised by OF and HL. KL, OF, and HL performed the fieldwork, and KL did the sampling. KL did the thermodynamic modeling with the help of PG, FP, and PL. PL and KL acquired the EPMA data. All authors took part in the discussion about the results, helped to improve the discussion, and participated in writing the paper.

Competing interests. The contact author has declared that none of the authors has any competing interests.

Special issue statement. This article is part of the special issue "(Ultra)high-pressure metamorphism, from crystal to orogenic scale". It is a result of the 14th International Eclogite Conference (IEC-14) held in Paris and Lyon, France, 10–13 July 2022.

Acknowledgements. Guy Libourel and Clément Ganino are thanked for fruitful discussions and access to preliminary SEM analyses at the Observatoire de la Côte d'Azur. We thank Solenn Hertgen for her help and discussion in the field. This work was partly supported by the French Renatech network and its FEMTO-ST technological facility. We thank Besim Dragovic, Sebastian Weber, and the anonymous reviewer for their constructive comments as well as Samuel Angiboust and Christian Chopin, whose comments and careful editorial handling helped improve the manuscript.

Financial support. The research was supported by the OSU THETA SRO (2021) project and the French National Centre for Scientific Research (CNRS-INSU) through their TelluS-ALEAS program (2021–2022) (funding granted to Olivier Fabbri). This publication was supported by the SFMC publication funding program (funding granted to Kilian Lecacheur).

Review statement. This paper was edited by Samuel Angiboust and reviewed by Besim Dragovic, Sebastian Weber, and one anonymous referee.

References

Ague, J. J.: Mass transfer during Barrovian metamorphism of pelites, south-central Connecticut. II: Channelized fluid flow and the growth of staurolite and kyanite, Am. J. Sci., 294, 1061–1134, https://doi.org/10.2475/ajs.294.9.1061, 1994.

Ague, J. J.: Extreme channelization of fluid and the problem of element mobility during Barrovian metamorphism, Am. Mineral., 96, 333–352, https://doi.org/10.2138/am.2011.3582, 2011.

Ague, J. J.: Fluid Flow in the Deep Crust, in: Treatise on Geochemistry: Second Edition, vol. 4, Elsevier, 203–247, https://doi.org/10.1016/B978-0-08-095975-7.00306-5, 2013.

Ague, J. J. and Carlson, W. D.: Metamorphism as garnet sees it: The kinetics of nucleation and growth, equilibration, and diffusional relaxation, Elements, 9, 439–445, https://doi.org/10.2113/gselements.9.6.439, 2013.

Ague, J. J. and Nicolescu, S.: Carbon dioxide released from subduction zones by fluid-mediated reactions, Nat. Geosci., 7, 355–360, https://doi.org/10.1038/ngeo2143, 2014.

Ague, J. J. and Van Haren, J. L. M.: Assessing metasomatic mass and volume changes using the bootstrap, with application to deep crustal hydrothermal alteration of marble, Econ. Geol., 91, 1169–1182, https://doi.org/10.2113/gsecongeo.91.7.1169, 1996.

Amato, J. M., Johnson, C. M., Baumgartner, L. P., and Beard, B. L.: Rapid exhumation of the Zermatt–Saas ophiolite deduced from high-precision Sm–Nd and Rb–Sr geochronology, Earth Planet. Sc. Lett., 171, 425–438, https://doi.org/10.1016/S0012-821X(99)00161-2, 1999.

Angiboust, S. and Agard, P.: Initial water budget: The key to detaching large volumes of eclogitized oceanic crust along the subduction channel?, Lithos, 120, 453–474, https://doi.org/10.1016/j.lithos.2010.09.007, 2010.

Angiboust, S., Agard, P., Jolivet, L., and Beyssac, O.: The Zermatt-Saas ophiolite: the largest (60-km wide) and deepest (c. 70–80 km) continuous slice of oceanic lithosphere detached from a subduction zone?, Terra Nova, 21, 171–180, https://doi.org/10.1111/j.1365-3121.2009.00870.x, 2009.

Angiboust, S., Agard, P., Raimbourg, H., Yamato, P., and Huet, B.: Subduction interface processes recorded by eclogite-facies shear zones (Monviso, W. Alps), Lithos, 127, 222–238, https://doi.org/10.1016/j.lithos.2011.09.004, 2011.

Angiboust, S., Agard, P., Yamato, P., and Raimbourg, H.: Eclogite breccias in a subducted ophiolite: A record of intermediate-depth earthquakes?, Geology, 40, 707–710, https://doi.org/10.1130/G32925.1, 2012a.

Angiboust, S., Langdon, R., Agard, P., Waters, D., and Chopin, C.: Eclogitization of the Monviso ophiolite (W. Alps) and implications on subduction dynamics, J. Metamorph. Geol., 30, 37–61, https://doi.org/10.1111/j.1525-1314.2011.00951.x, 2012b.

Angiboust, S., Pettke, T., De Hoog, J. C. M., Caron, B., and Oncken, O.: Channelized fluid flow and eclogite-facies metasomatism along the subduction shear zone, J. Petrol., 55, 883–916, https://doi.org/10.1093/petrology/egu010, 2014a.

Angiboust, S., Glodny, J., Oncken, O., and Chopin, C.: In search of transient subduction interfaces in the Dent Blanche–Sesia Tectonic System (W. Alps), Lithos, 205, 298–321, https://doi.org/10.1016/j.lithos.2014.07.001, 2014b.

Angiboust, S., Yamato, P., Hertgen, S., Hyppolito, T., Bebout, G. E., and Morales, L.: Fluid pathways and high-P metasomatism in a subducted continental slice (Mt. Emilius klippe, W. Alps), J. Metamorph. Geol., 35, 471–492, https://doi.org/10.1111/jmg.12241, 2017.

Atherton, M. P.: The Variation in Garnet, Biotite and Chlorite Composition in Medium Grade Pelitic Rocks from the Dalradian, Scotland, with Particular Reference to the Zonation in Garnet, Contrib. Mineral. Petr., 18, 347–371, https://doi.org/10.1007/BF00399696, 1968.

Ayers, J. C. and Watson, E. B.: Solubility of apatite, monazite, zircon, and rutile in supercritical aqueous fluids with implications for subduction zone geochemistry, Philos. T. Roy. Soc. A, 335, 365–375, https://doi.org/10.1098/rsta.1991.0052, 1991.

Bach, W. and Klein, F.: The petrology of seafloor rodingites: insights from geochemical reaction path modeling, Lithos, 112, 103–117, https://doi.org/10.1016/j.lithos.2008.10.022, 2009.

Ballèvre, M., Kienast, J.-R., and Vuichard, J.-P.: La "nappe de la Dent-Blanche" (Alpes occidentales): deux unités austroalpines indépendantes, Eclogae Geol. Helv., 79, 57–74, 1986.

Barnicoat, A. C. and Fry, N.: High-pressure metamorphism of the Zermatt-Saas ophiolite zone, Switzerland, J. Geol. Soc. London, 143, 607–618, https://doi.org/10.1144/gsjgs.143.4.0607, 1986.

Bearth, P.: Die Ophiolithe der Zone von Zermatt-Saas Fee, Beiträge zur Geol. Karte der Schweiz, 132, 130, 1967.

Bebout, G. E.: Metasomatism in Subduction Zones of Subducted Oceanic Slabs, Mantle Wedges, and the Slab-Mantle Interface, in: Lecture Notes in Earth System Sciences, vol. 0, Springer International Publishing, 289–349, https://doi.org/10.1007/978-3-642-28394-9_9, 2013.

Bebout, G. E. and Barton, M. D.: Metasomatism during subduction: products and possible paths in the Catalina Schist, California, Chem. Geol., 108, 61–92, https://doi.org/10.1016/0009-2541(93)90318-D, 1993.

Bebout, G. E. and Barton, M. D.: Tectonic and metasomatic mixing in a high-T, subduction-zone mélange–insights into the geochemical evolution of the slab–mantle interface, Chem. Geol., 187, 79–106, https://doi.org/10.1016/S0009-2541(02)00019-0, 2002.

Bedford, J., Fusseis, F., Leclère, H., Wheeler, J., and Faulkner, D.: A 4D view on the evolution of metamorphic dehydration reactions, Sci. Rep., 7, 1–7, https://doi.org/10.1038/s41598-017-07160-5, 2017.

Beinlich, A., Klemd, R., John, T., and Gao, J.: aTrace-element mobilization during Ca-metasomatism along a major fluid conduit: Eclogitization of blueschist as a consequence of fluid–rock interaction, Geochim. Cosmochim. Ac., 74, 1892–1922, https://doi.org/10.1016/j.gca.2009.12.011, 2010.

Beltrando, M., Manatschal, G., Mohn, G., Dal Piaz, G. V., Vitale-Brovarone, A., and Masini, E.: Recognizing remnants ofmagma-poor rifted margins in high-pressure orogenic belts: The Alpine case study, Earth-Sci. Rev., 131, 88–115, https://doi.org/10.1016/j.earscirev.2014.01.001, 2014.

Bovay, T., Rubatto, D., and Lanari, P.: Pervasive fluid-rock interaction in subducted oceanic crust revealed by oxygen isotope zoning in garnet, Contrib. Mineral. Petr., 176, 55, https://doi.org/10.1007/s00410-021-01806-4, 2021.

Bovay, T., Lanari, P., Rubatto, D., Smit, M., and Piccoli, F.: Pressure–temperature–time evolution of subducted crust revealed by complex garnet zoning (Theodul Glacier Unit, Switzerland), J. Metamorph. Geol., 40, 175–206, https://doi.org/10.1111/jmg.12623, 2022.

Bowtell, S. A., Cliff, R. A., and Barnicoat, A. C.: Sm-Nd isotopic evidence on the age of eclogitization in the Zermatt-Saas ophiolite, J. Metamorph. Geol., 12, 187–196, https://doi.org/10.1111/j.1525-1314.1994.tb00013.x, 1994.

Brandt, S. and Schenk, V.: Metamorphic Response to Alpine Thrusting of a Crustal-scale Basement Nappe in Southern Calabria (Italy), J. Petrol., 61, 1–39, https://doi.org/10.1093/petrology/egaa063, 2020.

Breeding, C. M., Ague, J. J., and Bröcker, M.: Fluid–metasedimentary rock interactions in subduction-zone mélange: Implications for the chemical composition of arc magmas, Geology, 32, 1041–1044, https://doi.org/10.1130/G20877.1, 2004.

Bretscher, A., Hermann, J., and Pettke, T.: The influence of oceanic oxidation on serpentinite dehydration during subduction, Earth Planet. Sc. Lett., 499, 173–184, https://doi.org/10.1016/j.epsl.2018.07.017, 2018.

Broadwell, K. S., Locatelli, M., Verlaguet, A., Agard, P., and Caddick, M. J.: Transient and periodic brittle deformation of eclogites during intermediate-depth subduction, Earth Planet. Sc. Lett., 521, 91–102, https://doi.org/10.1016/j.epsl.2019.06.008, 2019.

Bucher, K., Fazis, Y., de Capitani, C., and Grapes, R.: Blueschists, eclogites, and decompression assemblages of the Zermatt-Saas ophiolite: High-pressure metamorphism of subducted Tethys lithosphere, Am. Mineral., 90, 821–835, https://doi.org/10.2138/am.2005.1718, 2005.

Caddick, M. J., Konopásek, J., and Thompson, A. B.: Preservation of garnet growth zoning and the duration of prograde metamorphism, J. Petrol., 51, 2327–2347, https://doi.org/10.1093/petrology/egq059, 2010.

Cannat, M., Fontaine, F., and Escartín, J.: Serpentinization and associated hydrogen and methane fluxes at slow spreading ridges, in: Diversity of Hydrothermal Systems on Slow Spreading Ocean Ridges, AGU, 241–264, https://doi.org/10.1029/2008GM000760, 2010.

Carlson, W. D. and Gordon, C. L.: Effects of matrix grain size on the kinetics of intergranular diffusion, J. Metamorph. Geol., 22, 733–742, https://doi.org/10.1111/j.1525-1314.2004.00545.x, 2004.

Carmichael, I. S.: Igneous petrology, Igneous Petrol., https://doi.org/10.1016/0377-0273(85)90080-0, 1974.

Cartwright, I. and Barnicoat, A. C.: Petrology, geochronology, and tectonics of shear zones in the Zermatt–Saas and Combin zones of the Western Alps, J. Metamorph. Geol., 20, 263–281, https://doi.org/10.1046/J.0263-4929.2001.00366.X, 2002.

Coleman, R. G.: Low-temperature reaction zones and alpine ultramafic rocks of California, Oregon, and Washington, Geol. Surv. Bull., 1247, 46, 1967.

Connolly, J. A. D.: Computation of phase equilibria by linear programming: a tool for geodynamic modeling and its application to subduction zone decarbonation, Earth Planet. Sc. Lett., 236, 524–541, https://doi.org/10.1016/j.epsl.2005.04.033, 2005.

Connolly, J. A. D.: The mechanics of metamorphic fluid expulsion, Elements, 6, 165–172, https://doi.org/10.2113/gselements.6.3.165, 2010.

Connolly, J. A. D. and Galvez, M. E.: Electrolytic fluid speciation by Gibbs energy minimization and implications for subduction zone mass transfer, Earth Planet. Sc. Lett., 501, 90–102, https://doi.org/10.1016/j.epsl.2018.08.024, 2018.

Connolly, J. A. D. and Podladchikov, Y. Y.: Decompaction weakening and channeling instability in ductile porous media: Implications for asthenospheric melt segregation, J. Geophys. Res.-Sol. Ea., 112, 10205, https://doi.org/10.1029/2005JB004213, 2007.

Cygan, R. T. and Lasaga, A. C.: Crystal growth and the formation of chemical zoning in garnets, Contrib. Mineral. Petr., 79, 187–200, https://doi.org/10.1007/BF01132887, 1982.

Dai, J. G., Wang, C. S., Liu, S. A., Qian, X. Y., Zhu, D. C., and Ke, S.: Deep carbon cycle recorded by calcium-silicate rocks (rodingites) in a subduction-related ophiolite, Geophys. Res. Lett., 43, 11635–11643, https://doi.org/10.1002/2016GL070474, 2016.

Dal Piaz, G., Cortiana, G., Del Moro, A., Martin, S., Pennacchioni, G., and Tartarotti, P.: Tertiary age and paleostructural inferences of the eclogitic imprint in the Austroalpine outliers and Zermatt-Saas ophiolite, Western Alps, Int. J. Earth Sci., 90, 668–684, https://doi.org/10.1007/s005310000177, 2001.

Dal Piaz, G. V. and Nervo, R.: Il lembo di ricoprimento del Glacier-Rafray (Dent Blanche s.l.), Boll. Soc. Geol. Ital., 90, 401–414, 1971.

Deschamps, F., Godard, M., Guillot, S., and Hattori, K.: Geochemistry of subduction zone serpentinites: A review, Lithos, 178, 96–127, https://doi.org/10.1016/j.lithos.2013.05.019, 2013.

Dragovic, B., Angiboust, S., and Tappa, M. J.: Petrochronological close-up on the thermal structure of a paleo-subduction zone (W. Alps), Earth Planet. Sc. Lett., 547, 116446, https://doi.org/10.1016/j.epsl.2020.116446, 2020.

Dziggel, A., Wulff, K., Kolb, J., Meyer, F. M., and Lahaye, Y.: Significance of oscillatory and bell-shaped growth zoning in hydrothermal garnet: Evidence from the Navachab gold deposit, Namibia, Chem. Geol., 262, 262–276, https://doi.org/10.1016/j.chemgeo.2009.01.027, 2009.

Ellero, A. and Loprieno, A.: Nappe stack of Piemonte–Ligurian units south of Aosta Valley: New evidence from Urtier Valley (Western Alps), Geol. J., 53, 1665–1684, https://doi.org/10.1002/gj.2984, 2018.

Engi, M., Giuntoli, F., Lanari, P., Burn, M., Kunz, B., and Bouvier, A. S.: Pervasive Eclogitization Due to Brittle Deformation and Rehydration of Subducted Basement: Effects on Continental Recycling?, Geochem. Geophy. Geosy., 19, 865–881, https://doi.org/10.1002/2017GC007215, 2018.

Ernst, W. G. and Dal Piaz, G. V.: Mineral parageneses of eclogitic rocks and related mafic schists of the Piemonte ophiolite nappe, Breuil-St. Jacques area, Italian Western Alps, Am. Mineral., 63, 621–640, 1978.

Evans, T. P.: A method for calculating effective bulk composition modification due to crystal fractionation in garnet-bearing schist: implications for isopleth thermobarometry, J. Metamorph. Geol., 22, 547–557, https://doi.org/10.1111/j.1525-1314.2004.00532.x, 2004.

Faccenda, M., Gerya, T. V., Mancktelow, N. S., and Moresi, L.: Fluid flow during slab unbending and dehydration: Implications for intermediate-depth seismicity, slab weakening and deep water recycling, Geochem. Geophy. Geosy., 13, 8170, https://doi.org/10.1029/2011GC003860, 2012.

Fassmer, K., Obermüller, G., Nagel, T. J., Kirst, F., Froitzheim, N., Sandmann, S., Miladinova, I., Fonseca, R. O. C., and Münker, C.: High-pressure metamorphic age and significance of eclogite-facies continental fragments associated with oceanic lithosphere in the Western Alps (Etirol-Levaz Slice, Valtournenche, Italy), Lithos, 252–253, 145–159, https://doi.org/10.1016/j.lithos.2016.02.019, 2016.

Fazio, E., Cirrincione, R., and Pezzino, A.: Garnet crystal growth in sheared metapelites (southern Calabria-Italy): Relationships between isolated porphyroblasts and coalescing euhedral crystals, Period. Mineral., 78, 3–18, https://doi.org/10.2451/2009PM0001, 2009.

Feenstra, A., Petrakakis, K., and Rhede, D.: Variscan relicts in Alpine high-P pelitic rocks from Samos (Greece): evidence from multi-stage garnet and its included minerals, J. Metamorph. Geol., 25, 1011–1033, https://doi.org/10.1111/j.1525-1314.2007.00741.x, 2007.

Ferry, J. M. and Gerdes, M. L.: Chemically reactive fluid flow during metamorphism, Annu. Rev. Earth Planet. Sc., 26, 255–287, https://doi.org/10.1146/annurev.earth.26.1.255, 1998.

Fontana, E., Panseri, M., and Tartarotti, P.: Oceanic relict textures in the Mount Avic serpentinites, Western Alps, Ofioliti, 33, 105–118, 2008.

Fontana, E., Tartarotti, P., Panseri, M., and Buscemi, S.: Geological map of the Mount Avic massif (Western Alps Ophiolites), J. Maps, 11, 126–135, https://doi.org/10.1080/17445647.2014.959567, 2015.

Frost, R. B.: Contact metamorphism of serpentinite, chloritic blackwall and rodingite at Paddy-Go-Easy Pass, Central Cascades, Washington, J. Petrol., 16, 272–313, https://doi.org/10.1093/petrology/16.2.272, 1975.

Frost, R. B. and Beard, J. S.: On Silica Activity and Serpentinization, J. Petrol., 48, 1351–1368, https://doi.org/10.1093/petrology/egm021, 2007.

Gaidies, F., Morneau, Y. E., Petts, D. C., Jackson, S. E., Zagorevski, A., and Ryan, J. J.: Major and trace element mapping of garnet: Unravelling the conditions, timing and rates of metamorphism of the Snowcap assemblage, west-central Yukon, J. Metamorph. Geol., 39, 133–164, https://doi.org/10.1111/jmg.12562, 2021.

García-Casco, A., Torres-Roldán, R. L., Millán, G., Monié, P., and Schneider, J.: Oscillatory zoning in eclogitic garnet and amphibole, Northern Serpentinite Melange, Cuba: A record of tectonic instability during subduction?, J. Metamorph. Geol., 20, 581–598, https://doi.org/10.1046/j.1525-1314.2002.00390.x, 2002.

Gasco, I., Gattiglio, M., and Borghi, A.: Lithostratigraphic setting and P-T metamorphic evolution for the Dora Maira Massif along the Piedmont Zone boundary (middle Susa Valley, NW Alps), Int. J. Earth Sci., 100, 1065–1085, https://doi.org/10.1007/s00531-011-0640-8, 2011.

Gerrits, A. R., Inglis, E., Dragovic, B., Starr, P. G., Baxter, E. F., and Burton, K. W.: Tracing the source of oxidizing fluids in subduction zones using iron isotopes in garnet, Nat. Geosci., 12, 1029–1033, https://doi.org/10.1038/s41561-019-0471-y, 2019.

Gilio, M., Scambelluri, M., Agostini, S., Godard, M., Pettke, T., Agard, P., Locatelli, M., and Angiboust, S.: Fingerprinting and relocating tectonic slices along the plate interface: Evidence from the Lago Superiore unit at Monviso (Western Alps), Lithos, 352–353, 105308, https://doi.org/10.1016/j.lithos.2019.105308, 2020.

Giuntoli, F., Lanari, P., and Engi, M.: Deeply subducted continental fragments – Part 1: Fracturing, dissolution–precipitation, and diffusion processes recorded by garnet textures of the central Sesia Zone (western Italian Alps), Solid Earth, 9, 167–189, https://doi.org/10.5194/se-9-167-2018, 2018a.

Giuntoli, F., Lanari, P., Burn, M., Kunz, B. E., and Engi, M.: Deeply subducted continental fragments – Part 2: Insight from petrochronology in the central Sesia Zone (western Italian Alps), Solid Earth, 9, 191–222, https://doi.org/10.5194/se-9-191-2018, 2018b.

Giuntoli, F., Vitale-Brovarone, A., and Menegon, L.: feedback between high-pressure genesis of abiotic methane and strain localization in subducted carbonate rocks, Sci. Rep., 101, 1–15, https://doi.org/10.1038/s41598-020-66640-3, 2020.

Green, E. C. R., White, R. W., Diener, J. F. A., Powell, R., Holland, T. J. B., and Palin, R. M.: Activity–composition relations for the calculation of partial melting equilibria in metabasic rocks, J. Metamorph. Geol., 34, 845–869, https://doi.org/10.1111/jmg.12211, 2016.

Groppo, C., Beltrando, M., and Compagnoni, R.: The P–T path of the ultra-high pressure Lago Di Cignana and adjoining high-

pressure meta-ophiolitic units: insights into the evolution of the subducting Tethyan slab, J. Metamorph. Geol., 27, 207–231, https://doi.org/10.1111/j.1525-1314.2009.00814.x, 2009.

Gyomlai, T., Agard, P., Marschall, H. R., Jolivet, L., and Gerdes, A.: Metasomatism and deformation of block-in-matrix structures in Syros: The role of inheritance and fluid-rock interactions along the subduction interface, Lithos, 386–387, 105996, https://doi.org/10.1016/j.lithos.2021.105996, 2021.

Hacker, B. R., Peacock, S. M., Abers, G. A., and Holloway, S. D.: Subduction factory 2. Are intermediate-depth earthquakes in subducting slabs linked to metamorphic dehydration reactions?, J. Geophys. Res.-Sol. Ea., 108, 2030, https://doi.org/10.1029/2001jb001129, 2003.

Halama, R., John, T., Herms, P., Hauff, F., and Schenk, V.: A stable (Li, O) and radiogenic (Sr, Nd) isotope perspective on metasomatic processes in a subducting slab, Chem. Geol., 281, 151–166, https://doi.org/10.1016/j.chemgeo.2010.12.001, 2011.

Haws, A. A., Starr, P. G., Dragovic, B., Scambelluri, M., Belmonte, D., Caddick, M. J., Broadwell, K. S., Ague, J. J., and Baxter, E. F.: Meta-rodingite dikes as recorders of subduction zone metamorphism and serpentinite dehydration: Voltri Ophiolite, Italy, Chem. Geol., 565, 120077, https://doi.org/10.1016/j.chemgeo.2021.120077, 2021.

Hermann, J. and Rubatto, D.: Accessory phase control on the trace element signature of sediment melts in subduction zones, Chem. Geol., 265, 512–526, https://doi.org/10.1016/j.chemgeo.2009.05.018, 2009.

Herms, P., John, T., Bakker, R. J., and Schenk, V.: Evidence for channelized external fluid flow and element transfer in subducting slabs (Raspas Complex, Ecuador), Chem. Geol., 310–311, 79–96, https://doi.org/10.1016/j.chemgeo.2012.03.023, 2012.

Hertgen, S., Yamato, P., Morales, L. F. G., and Angiboust, S.: Evidence for brittle deformation events at eclogite-facies P-T conditions (example of the Mt. Emilius klippe, Western Alps), Tectonophysics, 706–707, 1–13, https://doi.org/10.1016/j.tecto.2017.03.028, 2017.

Herviou, C. and Bonnet, G.: Paleocene-Eocene High-Pressure Carbonation of Western Alps Serpentinites: Positive Feedback Between Deformation and CO_2-CH_4 Fluid Ingression Responsible for Slab Slicing?, Geochem. Geophy. Geosy., 24, e2022GC010557, https://doi.org/10.1029/2022GC010557, 2023.

Herwartz, D., Nagel, T. J., Münker, C., Scherer, E. E., and Froitzheim, N.: Tracing two orogenic cycles in one eclogite sample by Lu–Hf garnet chronometry, Nat. Geosci., 4, 178–183, https://doi.org/10.1038/ngeo1060, 2011.

Holland, T. and Powell, R.: Activity–composition relations for phases in petrological calculations: an asymmetric multicomponent formulation, Contrib. Mineral. Petr., 145, 492–501, https://doi.org/10.1007/s00410-003-0464-z, 2003.

Holland, T. J. B. and Powell, R.: An internally consistent thermodynamic data set for phases of petrological interest, J. Metamorph. Geol., 16, 309–343, https://doi.org/10.1111/j.1525-1314.1998.00140.x, 1998.

Holland, T. J. B. and Powell, R.: An improved and extended internally consistent thermodynamic dataset for phases of petrological interest, involving a new equation of state for solids, J. Metamorph. Geol., 29, 333–383, https://doi.org/10.1111/j.1525-1314.2010.00923.x, 2011.

Hollister, L. S.: Garnet zoning: an interpretation based on the Rayleigh fractionation model, Science, 154, 1647–1651, https://doi.org/10.1126/science.154.3757.1647, 1966.

Hoover, W. F., Penniston-Dorland, S., Baumgartner, L., Bouvier, A. S., Dragovic, B., Locatelli, M., Angiboust, S., and Agard, P.: Episodic fluid flow in an eclogite-facies shear zone: Insights from Li isotope zoning in garnet, Geology, 50, 746–750, https://doi.org/10.1130/G49737.1, 2022.

Hyndman, R. D. and Peacock, S. M.: Serpentinization of the forearc mantle, Earth Planet. Sc. Lett., 212, 417–432, https://doi.org/10.1016/S0012-821X(03)00263-2, 2003.

Hyppolito, T., Cambeses, A., Angiboust, S., Raimondo, T., García-Casco, A., and Juliani, C.: Rehydration of eclogites and garnet-replacement processes during exhumation in the amphibolite facies, in: Geological Society Special Publication, 478, 217–239, https://doi.org/10.1144/SP478.3, 2019.

Jochum, K. P., Weis, U., Schwager, B., Stoll, B., Wilson, S. A., Haug, G. H., Andreae, M. O., and Enzweiler, J.: Reference Values Following ISO Guidelines for Frequently Requested Rock Reference Materials, Geostand. Geoanal. Res., 40, 333–350, https://doi.org/10.1111/j.1751-908X.2015.00392.x, 2016.

John, T. and Schenk, V.: Partial eclogitisation of gabbroic rocks in a late Precambrian subduction zone (Zambia): prograde metamorphism triggered by fluid infiltration, Contrib. Mineral. Petr., 146, 174–191, https://doi.org/10.1007/s00410-003-0492-8, 2003.

Kempf, E. D., Hermann, J., Reusser, E., Baumgartner, L. P., and Lanari, P.: The role of the antigorite + brucite to olivine reaction in subducted serpentinites (Zermatt, Switzerland), Swiss J. Geosci., 113, 1–36, https://doi.org/10.1186/S00015-020-00368-0, 2020.

Kerrick, D. M. and Connelly, J. A. D.: Metamorphic devolatilization of subductedmarine sediments and the transport of volatiles into the Earth's mantle, Nature, 411, 293–296, https://doi.org/10.1038/35077056, 2001.

Konrad-Schmolke, M., Handy, M. R., Babist, J., and O'Brien, P. J.: Thermodynamic modelling of diffusion-controlled garnet growth, Contrib. Miner. Petrol., 149, 181–195, https://doi.org/10.1007/s00410-004-0643-6, 2005.

Konrad-Schmolke, M., Babist, J., Handy, M. R., and O'Brien, P. J.: The Physico-Chemical Properties of a Subducted Slab from Garnet Zonation Patterns (Sesia Zone, Western Alps), J. Petrol., 47, 2123–2148, https://doi.org/10.1093/petrology/egl039, 2006.

Konrad-Schmolke, M., O'Brien, P. J., and Heidelbach, F.: Compositional re-equilibration of garnet: the importance of sub-grain boundaries, Eur. J. Mineral., 19, 431–438, https://doi.org/10.1127/0935-1221/2007/0019-1749, 2007.

Konrad-Schmolke, M., O'Brien, P. J., de Capitani, C., and Carswell, D. A.: Garnet growth at high- and ultra-high pressure conditions and the effect of element fractionation on mineral modes and composition, Lithos, 103, 309–332, https://doi.org/10.1016/j.lithos.2007.10.007, 2008.

Kulhánek, J. and Faryad, S. W.: Compositional changes in garnet: trace element transfer during eclogite-facies metamorphism, Contrib. Mineral. Petr., 178, 1–31, https://doi.org/10.1007/s00410-023-02050-8, 2023.

Laborda-López, C., López-Sánchez-Vizcaíno, V., Marchesi, C., Gómez-Pugnaire, M. T., Garrido, C. J., Jabaloy-Sánchez, A., Padrón-Navarta, J. A., and Hidas, K.: High-P metamorphism of rodingites during serpentinite dehydration (Cerro del Almirez, Southern Spain): Implications for the redox state

in subduction zones, J. Metamorph. Geol., 36, 1141–1173, https://doi.org/10.1111/jmg.12440, 2018.

Lanari, P. and Duesterhoeft, E.: Modeling metamorphic rocks using equilibrium thermodynamics and internally consistent databases: Past achievements, problems and perspectives, J. Petrol., 60, 19–56, https://doi.org/10.1093/petrology/egy105, 2019.

Lanari, P. and Engi, M.: Local Bulk Composition Effects on Metamorphic Mineral Assemblages, Rev. Mineral. Geochem., 83, 55–102, https://doi.org/10.2138/rmg.2017.83.3, 2017.

Lanari, P., Vidal, O., De Andrade, V., Dubacq, B., Lewin, E., Grosch, E. G., and Schwartz, S.: XMapTools: A MATLAB©-based program for electron microprobe X-ray image processing and geothermobarometry, Comput. Geosci., 62, 227–240, https://doi.org/10.1016/j.cageo.2013.08.010, 2014.

Lanari, P., Vho, A., Bovay, T., Airaghi, L., and Centrella, S.: Quantitative compositional mapping of mineral phases by electron probe micro-analyser, in: Geological Society Special Publication, 478, Geological Society of London, 39–63, https://doi.org/10.1144/SP478.4, 2019.

Lecacheur, K., Fabbri, O., Piccoli, F., Lanari, P., Goncalves, P., and Leclère, H.: Data set: High-Pressure Ca metasomatism of metabasites (Monte Avic, Western Alps), dat@UBFC [data set], https://doi.org/10.25666/DATAUBFC-2024-07-18, 2024.

Lefeuvre, B., Agard, P., Verlaguet, A., Dubacq, B., and Plunder, A.: Massive formation of lawsonite in subducted sediments from the Schistes Lustrés (W. Alps): Implications for mass transfer and decarbonation in cold subduction zones, Lithos, 370–371, 105629, https://doi.org/10.1016/j.lithos.2020.105629, 2020.

Lemoine, M., Bas, T., Arnaud-Vanneau, A., Arnaud, H., Dumont, T., Gidon, M., Bourbon, M., de Graciansky, P. C., Rudkiewicz, J. L., Megard-Galli, J., and Tricart, P.: The continental margin of the Mesozoic Tethys in the Western Alps, Mar. Petrol. Geol., 3, 179–199, https://doi.org/10.1016/0264-8172(86)90044-9, 1986.

Li, J. L., John, T., Gao, J., Klemd, R., and Wang, X. S.: Subduction channel fluid–rock interaction andmass transfer: Constraints from a retrograde vein in blueschist (SW Tianshan, China), Chem. Geol., 456, 28–42, https://doi.org/10.1016/J.CHEMGEO.2017.03.003, 2017.

Li, X.-P., Rahn, M., and Bucher, K.: Metamorphic processes in rodingites of the Zermatt-Saas ophiolites, Int. Geol. Rev., 46, 28–51, https://doi.org/10.2747/0020-6814.46.1.28, 2004.

Li, X. P., Rahn, M., and Bucher, K.: Eclogite facies metarodingites – phase relations in the system SiO_2-Al_2O_3-Fe_2O_3-FeO-MgO-CaO-CO_2-H_2O: an example from the Zermatt-Saas ophiolite, J. Metamorph. Geol., 26, 347–364, https://doi.org/10.1111/j.1525-1314.2008.00761.x, 2008.

Locatelli, M., Verlaguet, A., Agard, P., Federico, L., and Angiboust, S.: Intermediate-depth brecciation along the subduction plate interface (Monviso eclogite, W. Alps), Lithos, 320–321, 378–402, https://doi.org/10.1016/j.lithos.2018.09.028, 2018.

Locatelli, M., Verlaguet, A., Agard, P., Pettke, T., and Federico, L.: Fluid pulses during stepwise brecciation at intermediate subduction depths (Monviso eclogites, W. Alps): first internally then externally sourced, Geochem. Geophy. Geosy., 20, 5285–5318, https://doi.org/10.1029/2019GC008549, 2019.

Lü, Z., Zhang, L., Du, J., and Bucher, K.: Petrology of coesite-bearing eclogite from Habutengsu Valley, western Tianshan, NW China and its tectonometamorphic implication, J. Metamorph. Geol., 27, 773–787, https://doi.org/10.1111/j.1525-1314.2009.00845.x, 2009.

Luoni, P., Zanoni, D., Rebay, G., and Spalla, M. I.: Deformation history of Ultra High-Pressure ophiolitic serpentinites in the Zermatt-Saas Zone, Créton, Upper Valtournanche (Aosta Valley, Western Alps), Ofioliti, 44, 111–123, https://doi.org/10.4454/ofioliti.v44i2.528, 2019.

Maggi, M., Rossetti, F., Ranalli, G., and Theye, T.: Feedback between fluid infiltration and rheology along a regional ductile-to-brittle shear zone: The East Tenda Shear Zone (Alpine Corsica), Tectonics, 33, 253–280, https://doi.org/10.1002/2013TC003370, 2014.

Malvoisin, B., Podladchikov, Y. Y., and Vrijmoed, J. C.: Coupling changes in densities and porosity to fluid pressure variations in reactive porous fluid flow: Local thermodynamic equilibrium, Geochem. Geophy. Geosy., 16, 4362–4387, https://doi.org/10.1002/2015GC006019, 2015.

Manning, C. E.: The chemistry of subduction-zone fluids, Earth Planet. Sc. Lett., 223, 1–16, https://doi.org/10.1016/J.EPSL.2004.04.030, 2004.

Manzotti, P. and Ballèvre, M.: Multistage garnet in high-pressure metasediments: Alpine overgrowths on Variscan detrital grains, Geology, 41, 1151–1154, https://doi.org/10.1130/G34741.1, 2013.

Manzotti, P., Rubatto, D., Darling, J., Zucali, M., Cenki-Tok, B., and Engi, M.: From Permo-Triassic lithospheric thinning to Jurassic rifting at the Adriatic margin: Petrological and geochronological record in Valtournenche (Western Italian Alps), Lithos, 146–147, 276–292, https://doi.org/10.1016/j.lithos.2012.05.007, 2012.

Manzotti, P., Regis, D., Petts, D. C., Graziani, R., and Polivchuk, M.: Formation of multistage garnet grains by fragmentation and overgrowth constrained by microchemical and microstructural mapping, J. Metamorph. Geol., 42, 471–496, https://doi.org/10.1111/jmg.12761, 2024.

Martin, L. A. J., Rubatto, D., Vitale Brovarone, A., and Hermann, J.: Late Eocene lawsonite-eclogite facies metasomatism of a granulite sliver associated to ophiolites in Alpine Corsica, Lithos, 125, 620–640, https://doi.org/10.1016/j.lithos.2011.03.015, 2011.

Martin, L. A. J., Hermann, J., Gauthiez-Putallaz, L., Whitney, D. L., Vitale Brovarone, A., Fornash, K. F., and Evans, N. J.: Lawsonite geochemistry and stability–implication for trace element and water cycles in subduction zones, J. Metamorph. Geol., 32, 455–478, https://doi.org/10.1111/jmg.12093, 2014.

Martin, S., Rebay, G., Kienast, J. R., and Mével, C.: An eclogitic oceanic palaeo-hydrothermal field from the St. Marcel Valley, Ofioliti, 31, 49–63, 2008.

Menzel, M. D., Garrido, C. J., and López Sánchez-Vizcaíno, V.: Fluid-mediated carbon release from serpentinite-hosted carbonates during dehydration of antigorite-serpentinite in subduction zones, Earth Planet. Sc. Lett., 531, 115964, https://doi.org/10.1016/j.epsl.2019.115964, 2020.

Moore, S. J., Carlson, W. D., and Hesse, M. A.: Origins of yttrium and rare earth element distributions in metamorphic garnet, J. Metamorph. Geol., 31, 663–689, https://doi.org/10.1111/jmg.12039, 2013.

Muñoz-Montecinos, J., Angiboust, S., Garcia-Casco, A., Glodny, J., and Bebout, G.: Episodic hydrofracturing and large-scale flushing along deep subduction interfaces: Impli-

cations for fluid transfer and carbon recycling (Zagros Orogen, southeastern Iran), Chem. Geol., 571, 120173, https://doi.org/10.1016/j.chemgeo.2021.120173, 2021.

Nosenzo, F., Manzotti, P., and Robyr, M.: H_2O budget and metamorphic re-equilibration in polycyclic rocks as recorded by garnet textures and chemistry, Lithos, 452–453, https://doi.org/10.1016/j.lithos.2023.107230, 2023.

O'Hanley, D. S., Schandl, E. S., and Wicks, F. J.: The origin of rodingites from Cassiar, British Columbia, and their use to estimate T and P (H_2O) during serpentinization, Geochim. Cosmochim. Ac., 56, 97–108, https://doi.org/10.1016/0016-7037(92)90119-4, 1992.

Oliver, N. H. S.: Review and classification of structural controls on fluid flow during regional metamorphism, J. Metamorph. Geol., 14, 477–492, https://doi.org/10.1046/j.1525-1314.1996.00347.x, 1996.

Padrón-Navarta, J. A., Hermann, J., Garrido, C. J., López Sánchez-Vizcaíno, V., and Gómez-Pugnaire, M. T.: An experimental investigation of antigorite dehydration in natural silica-enriched serpentinite, Contrib. Mineral. Petr., 159, 25–42, https://doi.org/10.1007/s00410-009-0414-5, 2010.

Panseri, M., Fontana, E., and Tartarotti, P.: Evolution of rodingitic dykes: Metasomatism and metamorphism in the Mount Avic serpentinites (Alpine Ophiolites, southern Aosta Valley), Ofioliti, 33, 165–185, 2008.

Philippot, P.: "Crack seal" vein geometry in eclogitic rocks, Geodin. Acta, 1, 171–181, https://doi.org/10.1080/09853111.1987.11105136, 1987.

Philpotts, A. and Ague, J.: Principles of Igneous and Metamorphic Petrology, Cambridge University Press, https://doi.org/10.1017/cbo9780511813429, 2009.

Piccoli, F., Vitale Brovarone, A., Beyssac, O., Martinez, I., Ague, J. J., and Chaduteau, C.: Carbonation by fluid–rock interactions at high-pressure conditions: implications for carbon cycling in subduction zones, Earth Planet. Sc. Lett., 445, 146–159, https://doi.org/10.1016/j.epsl.2016.03.045, 2016.

Piccoli, F., Vitale Brovarone, A., and Ague, J. J.: Field and petrological study of metasomatism and high-pressure carbonation from lawsonite eclogite-facies terrains, Alpine Corsica, Lithos, 304–307, 16–37, https://doi.org/10.1016/j.lithos.2018.01.026, 2018.

Piccoli, F., Ague, J. J., Chu, X., Tian, M., and Vitale Brovarone, A.: Field-based evidence for intra-slab high-permeability channel formation at eclogite-facies conditions during subduction, Geochem. Geophy. Geosy., 22, 1–17, https://doi.org/10.1029/2020GC009520, 2021.

Plank, T. and Langmuir, C. H.: The chemical composition of subducting sediment and its consequences for the crust and mantle, Chem. Geol., 145, 325–394, https://doi.org/10.1016/S0009-2541(97)00150-2, 1998.

Plümper, O., John, T., Podladchikov, Y. Y., Vrijmoed, J. C., and Scambelluri, M.: Fluid escape from subduction zones controlled by channel-forming reactive porosity, Nat. Geosci., 10, 150–156, https://doi.org/10.1038/ngeo2865, 2017.

Pyle, J. M. and Spear, F. S.: Yttrium zoning in garnet: Coupling of major and accessory phases during metamorphic reactions, Geol. Mater. Res., 1, 1–49, 1999.

Raimondo, T., Payne, J., Wade, B., Lanari, P., Clark, C., and Hand, M.: Trace element mapping by LA-ICP-MS: assessing geochemical mobility in garnet, Contrib. Mineral. Petr., 172, 1–22, https://doi.org/10.1007/s00410-017-1339-z, 2017.

Rebay, G., Spalla, M. I., and Zanoni, D.: Interaction of deformation and metamorphism during subduction and exhumation of hydrated oceanic mantle: Insights from the Western Alps, J. Metamorph. Geol., 30, 687–702, https://doi.org/10.1111/j.1525-1314.2012.00990.x, 2012.

Reinecke, T.: Very-high-pressure metamorphism and uplift of coesite-bearing metasediments from the Zermatt-Saas zone, Western Alps, Eur. J. Mineral., 3, 7–18, https://doi.org/10.1127/ejm/3/1/0007, 1991.

Reinecke, T.: Prograde high- to ultrahigh-pressure metamorphism and exhumation of oceanic sediments at Lago di Cignana, Zermatt-Saas Zone, western Alps, Lithos, 42, 147–189, https://doi.org/10.1016/S0024-4937(97)00041-8, 1998.

Rogowitz, A., Thielmann, M., Kraus, K., Grasemann, B., and Renner, J.: The effect of the garnet content on deformation mechanisms and weakening of eclogite: Insights from deformation experiments and numerical simulations, Geochem. Geophy. Geosy., 24, e2022GC010743, https://doi.org/10.1029/2022GC010743, 2023.

Rotondo, F. C., Tartarotti, P., Guerini, S., Porta, G. D., and Campomenosi, N.: Metasomatic horizon sealing serpentinite-metasediments pair in the Zermatt-Saas metaophiolite (Northwestern Alps): Record of a channel for focussed fluid flow during subduction, Ofioliti, 46, 1–25, https://doi.org/10.4454/ofioliti.v46i1.535, 2021.

Rubatto, D. and Angiboust, S.: Oxygen isotope record of oceanic and high-pressure metasomatism: a P–T–time–fluid path for the Monviso eclogites (Italy), Contrib. Mineral. Petr., 170, 1–16, https://doi.org/10.1007/s00410-015-1198-4, 2015.

Rubatto, D., Gebauer, D., and Fanning, M.: Jurassic formation and Eocene subduction of the Zermatt–Saas-Fee ophiolites: implications for the geodynamic evolution of the Central and Western Alps, Contrib. Mineral. Petr., 132, 269–287, https://doi.org/10.1007/s004100050421, 1998.

Rubatto, D., Burger, M., Lanari, P., Hattendorf, B., Schwarz, G., Neff, C., Keresztes Schmidt, P., Hermann, J., Vho, A., and Günther, D.: Identification of growth mechanisms in metamorphic garnet by high-resolution trace element mapping with LA-ICP-TOFMS, Contrib. Mineral. Petr., 175, 1–19, https://doi.org/10.1007/s00410-020-01700-5, 2020.

Ruiz Cruz, M. D.: Origin of atoll garnet in schists from the Alpujárride complex (central zone of the Betic Cordillera, Spain): Implications on the P-T evolution, Mineral. Petrol., 101, 245–261, https://doi.org/10.1007/s00710-011-0147-9, 2011.

Rüpke, L. H., Morgan, J. P., Hort, M., and Connolly, J. A. D.: Serpentine and the subduction zone water cycle, Earth Planet. Sc. Lett., 223, 17–34, https://doi.org/10.1016/j.epsl.2004.04.018, 2004.

Sandmann, S., Nagel, T. J., Herwartz, D., Fonseca, R. O. C., Kurzawski, R. M., Münker, C., and Froitzheim, N.: Lu–Hf garnet systematics of a polymetamorphic basement unit: new evidence for coherent exhumation of the Adula Nappe (Central Alps) from eclogite-facies conditions, Contrib. Mineral. Petr., 168, 1–21, https://doi.org/10.1007/s00410-014-1075-6, 2014.

Scambelluri, M., Strating, E. H. H., Piccardo, G. B., Vissers, R. L. M., and Ramponr, E.: Alpine olivine- and titanian clinohumite-bearing assemblages in the Erro-Tobbio peridotite

(Voltri Massif, NW Italy), J. Metamorph. Geol., 9, 79–91, https://doi.org/10.1111/j.1525-1314.1991.tb00505.x, 1991.

Scambelluri, M., Muntener, O., Hermann, J., Piccardo, G. B., and Trommsdorff, V.: Subduction of water into the mantle: history of an Alpine peridotite, Geology, 23, 459–462, https://doi.org/10.1130/0091-7613(1995)023<0459:SOWITM>2.3.CO;2, 1995.

Scambelluri, M., Cannaò, E., Guerini, S., Bebout, G. E., Epstein, G. S., Rotondo, F., Campomenosi, N., and Tartarotti, P.: Carbon mobility and exchange in a plate-interface subduction mélange: A case study of meta-ophiolitic rocks in Champorcher Valley, Italian Alps, Lithos, 428–429, https://doi.org/10.1016/j.lithos.2022.106813, 2022.

Schandl, E. S., O'Hanley, D. S., Wicks, F. J., and Kyser, T. K.: Fluid inclusions in rodingite: A geothermometer for serpentinization, Econ. Geol., 85, 1273–1276, https://doi.org/10.2113/gsecongeo.85.6.1273, 1990.

Schmid, S. M., Fügenschuh, B., Kissling, E., and Schuster, R.: Tectonic map and overall architecture of the Alpine orogen, Eclogae Geol. Helv., 97, 93–117, https://doi.org/10.1007/s00015-004-1113-x, 2004.

Schmidt, M. W. and Poli, S.: Experimentally based water budgets for dehydrating slabs and consequences for arc magma generation, Earth Planet. Sc. Lett., 163, 361–379, https://doi.org/10.1016/S0012-821X(98)00142-3, 1998.

Schmidt, M. W. and Poli, S.: Devolatilization During Subduction, in: Treatise on Geochemistry: Second Edition, vol. 4, Elsevier, 669–701, https://doi.org/10.1016/B978-0-08-095975-7.00321-1, 2013.

Schumacher, R., Rötzler, K., and Maresch, W. V: Subtle oscillatory zoning in garnet from regional metamorphic Phyllites and Mica Schists, Western Erzgebirge, Germany, Can. Mineral., 37, 381–402, 1999.

Spandler, C., Pettke, T., and Rubatto, D.: Internal and external fluid sources for eclogite-facies veins in the Monviso Meta-ophiolite, Western Alps: Implications for fluid flow in subduction zones, J. Petrol., 52, 1207–1236, https://doi.org/10.1093/petrology/egr025, 2011.

Spear, F. S.: On the interpretation of peak metamorphic temperatures in light of garnet diffusion during cooling, J. Metamorph. Geol., 9, 379–388, https://doi.org/10.1111/j.1525-1314.1991.tb00533.x, 1991.

Tartarotti, P., Benciolini, L., and Monopoli, B.: Brecce serpentinitiche nel massiccio ultrabasico del Monte Avic (Falda Ofiolitica Piemontese): Possibili evidenze di erosione sottomarina, Atti Tic. Sc. Terra, 73–86 pp., 1998.

Tartarotti, P., Martin, S., Monopoli, B., Benciolini, L., Schiavo, A., Campana, R., Vigni, I., Desio, T. A., Dipartimento, M., Land, P., Services, S., Chimica, D., Servizio, U., Provincia, G., and Blanche, D.: Geological map of the St. Marcel Valley metaophiolites, 1000, 707–717, https://doi.org/10.1080/17445647.2017.1355853, 2017a.

Tartarotti, P., Martin, S., Monopoli, B., Benciolini, L., Schiavo, A., Campana, R., and Vigni, I.: Geology of the Saint-Marcel valley metaophiolites (Northwestern Alps, Italy), J. Maps, 13, 707–717, https://doi.org/10.1080/17445647.2017.1355853, 2017b.

Tartarotti, P., Festa, A., Benciolini, L., and Balestro, G.: Record of Jurassic mass transport processes through the orogenic cycle: Understanding chaotic rock units in the high-pressure Zermatt-Saas ophiolite (Western Alps), Lithosphere, 9, 399–407, https://doi.org/10.1130/L605.1, 2017c.

Tartarotti, P., Martin, S., Meyzen, C. M., Benciolini, L., and Toffolo, L.: Structural evolution and metasomatism of subducted metaophiolites in the Northwestern Alps, Tectonics, 38, 4185–4206, https://doi.org/10.1029/2019TC005626, 2019.

Thöni, M. and Miller, C.: The "Permian event" in the Eastern European Alps: Sm–Nd and P–T data recorded by multistage garnet from the Plankogel unit, Chem. Geol., 260, 20–36, https://doi.org/10.1016/j.chemgeo.2008.11.017, 2009.

Tsikouras, B., Karipi, S., Rigopoulos, I., Perraki, M., Pomonis, P., and Hatzipanagiotou, K.: Geochemical processes and petrogenetic evolution of rodingite dykes in the ophiolite complex of Othrys (Central Greece), Lithos, 113, 540–554, https://doi.org/10.1016/j.lithos.2009.06.013, 2009.

Tsujimori, T., Sisson, V. B., Liou, J. G., Harlow, G. E., and Sorensen, S. S.: Very-low-temperature record of the subduction process: A review of worldwide lawsonite eclogites, Lithos, 92, 609–624, https://doi.org/10.1016/j.lithos.2006.03.054, 2006.

Ulmer, P. and Trommsdorff, V.: Phase relations of hydrous mantle subducting to 300 km, Mantle Petrol. F. Obs. High-Pressure Exp. Spec. Publ. Geochem. Soc. No. 6, 259–281, 1999.

Van Der Klauw, S. N. G. C., Reinecke, T., and Stöckhert, B.: Exhumation of ultrahigh-pressure metamorphic oceanic crust from Lago di Cignana, Piemontese zone, western Alps: the structural record in metabasites, Lithos, 41, 79–102, https://doi.org/10.1016/s0024-4937(97)82006-3, 1997.

Van Keken, P. E., Hacker, B. R., Syracuse, E. M., and Abers, G. A.: Subduction factory: 4. Depth-dependent flux of H_2O from subducting slabs worldwide, J. Geophys. Res.-Sol. Ea., 116, 1401, https://doi.org/10.1029/2010JB007922, 2011.

Vho, A., Rubatto, D., Lanari, P., Giuntoli, F., Regis, D., and Jörg, H.: Crustal reworking and hydration: insights from element zoning and oxygen isotopes of garnet in high-pressure rocks (Sesia Zone, Western Alps), Contrib. Mineral. Petr., 175, 109, https://doi.org/10.1007/s00410-020-01745-6, 2020.

Viete, D. R., Hacker, B. R., Allen, M. B., Seward, G. G. E., Tobin, M. J., Kelley, C. S., Cinque, G., and Duckworth, A. R.: Metamorphic records of multiple seismic cycles during subduction, Sci. Adv., 4, 1–13, https://doi.org/10.1126/sciadv.aaq0234, 2018.

Vitale Brovarone, A. and Beyssac, O.: Lawsonite metasomatism: A new route for water to the deep Earth, Earth Planet. Sc. Lett., 393, 275–284, https://doi.org/10.1016/j.epsl.2014.03.001, 2014.

Vitale-Brovarone, A., Alard, O., Beyssac, O., Martin, L., and Picatto, M.: Lawsonite metasomatism and trace element recycling in subduction zones, J. Metamorph. Geol., 32, 489–514, https://doi.org/10.1111/jmg.12074, 2014.

Vitale-Brovarone, A., Martinez, I., Elmaleh, A., Compagnoni, R., Chaduteau, C., Ferraris, C., and Esteve, I.: Massive production of abiotic methane during subduction evidenced in metamorphosed ophicarbonates from the Italian Alps, Nat. Commun., 81, 1–13, https://doi.org/10.1038/ncomms14134, 2017.

Weber, S. and Bucher, K.: An eclogite-bearing continental tectonic slice in the Zermatt-Saas high-pressure ophiolites at Trockener Steg (Zermatt, Swiss Western Alps), Lithos, 232, 336–359, https://doi.org/10.1016/j.lithos.2015.07.010, 2015.

Weber, S., Hauke, M., Martinez, R. E., Redler, C., Münker, C., and Froitzheim, N.: Fluid-driven transformation of blueschist to vein eclogite during the Early Eocene in a subducted sliver of con-

tinental crust (Monte Emilius, Italian Western Alps), J. Metamorph. Geol., 40, 553–584, https://doi.org/10.1111/jmg.12638, 2022.

White, R. W., Powell, R., Holland, T. J. B., and Worley, B.: The effect of TiO_2 and Fe_2O_3 on metapelitic assemblages at greenschist and amphibolite facies conditions: Mineral equilibria calculations in the system K_2O-FeO-MgO-Al_2O_3-SiO_2-H_2O-TiO_2-Fe_2O_3, J. Metamorph. Geol., 18, 497–511, https://doi.org/10.1046/j.1525-1314.2000.00269.x, 2000.

White, R. W., Powell, R., Holland, T. J. B., Johnson, T. E., and Green, E. C. R.: New mineral activity-composition relations for thermodynamic calculations in metapelitic systems, J. Metamorph. Geol., 32, 261–286, https://doi.org/10.1111/jmg.12071, 2014.

Wilson, C. R., Spiegelman, M., van Keken, P. E., and Hacker, B. R.: Fluid flow in subduction zones: The role of solid rheology and compaction pressure, Earth Planet. Sc. Lett., 401, 261–274, https://doi.org/10.1016/j.epsl.2014.05.052, 2014.

Woodcock, N. H. and Mort, K.: Classification of fault breccias and related fault rocks: Geological Magazine, 175, 435–440, https://doi.org/10.1017/S0016756808004883, 2008.

Yamato, P., Duretz, T., and Angiboust, S.: Brittle/Ductile Deformation of Eclogites: Insights From Numerical Models, Geochem. Geophy. Geosy., 20, 3116–3133, https://doi.org/10.1029/2019GC008249, 2019.

Yang, P. and Pattison, D.: Genesis of monazite and Y zoning in garnet from the Black Hills, South Dakota, Lithos, 88, 233–253, https://doi.org/10.1016/j.lithos.2005.08.012, 2006.

Zack, T. and John, T.: An evaluation of reactive fluid flow and trace element mobility in subducting slabs, Chem. Geol., 239, 199–216, https://doi.org/10.1016/j.chemgeo.2006.10.020, 2007.

Zanoni, D., Rebay, G., and Spalla, M. I.: Ocean floor and subduction record in the Zermatt-Saas rodingites, Valtournanche, Western Alps, J. Metamorph. Geol., 34, 941–961, https://doi.org/10.1111/jmg.12215, 2016.